Aging Cell
Open Access

Monoamine oxidase-A is a novel driver of stress-induced premature senescence through inhibition of parkin-mediated mitophagy

Journal:	*Aging Cell*
Manuscript ID	Draft
Manuscript Type:	Original Paper
Date Submitted by the Author:	n/a
Complete List of Authors:	Manzella, Nicola; INSERM institute of Metabolic and Cardiovascular Diseases, cardiology Maggiorani, Damien; INSERM institute of Metabolic and Cardiovascular Diseases, cardiology Santin, Yohan; INSERM institute of Metabolic and Cardiovascular Diseases, cardiology Martini, Hélène; INSERM institute of Metabolic and Cardiovascular Diseases, cardiology Douin-Echinard, Victorine; INSERM institute of Metabolic and Cardiovascular Diseases, cardiology Passos, Joao; Newcastle University Institute for Ageing and Health, Ageing research laboratories Lezoualc'h, Frank; INSERM institute of Metabolic and Cardiovascular Diseases, cardiology Binda, Claudia; Universita degli Studi di Pavia Dipartimento di Biologia e Biotecnologie Lazzaro Spallanzani, biology and biotechnology Parini, Angelo; INSERM institute of Metabolic and Cardiovascular Diseases, cardiology Mialet-Perez, jeanne; INSERM institute of Metabolic and Cardiovascular Diseases, cardiology
Keywords:	accelerated aging, cellular senescence, mitochondria, reactive oxygen species, autophagy

SCHOLARONE™
Manuscripts

Monoamine oxidase-A is a novel driver of stress-induced premature senescence through inhibition of parkin-mediated mitophagy

Nicola Manzella[1,2], Damien Maggiorani[1], Yohan Santin[1], Hélène Martini[1], Victorine Douin-Echinard[1], Joao F. Passos[3], Frank Lezoualc'h[1], Claudia Binda[2], Angelo Parini[1] and Jeanne Mialet-Perez[1]

[1]Institute of Metabolic and Cardiovascular Diseases (I2MC), Institut National de la Santé et de la Recherche Médicale (INSERM), Université de Toulouse, Toulouse, France

[2]Department of Biology and Biotechnology, University of Pavia, Via Ferrata 1, 27100 Pavia, Italy

[3]Ageing Research Laboratories, Newcastle University Institute for Ageing, Newcastle University, Newcastle upon Tyne NE4 5PL, UK

Corresponding author:
Jeanne Mialet-Perez, PhD
INSERM, Institut des Maladies Métaboliques et Cardiovasculaires
1 Avenue Jean Poulhès, BP 84225
31432 Toulouse Cedex 4, FRANCE
Tel. (33) 5 61 32 56 43
Fax. (33) 5 61 32 56 22
E-mail: jeanne.perez@inserm.fr

nicolamanzella@virgilio.it, damien.maggiorani@inserm.fr, yohan.santin@inserm.fr, helene.martini@inserm.fr, victorine.douin@inserm.fr, joao.passos@newcastle.ac.uk, frank.lezoualch@inserm.fr, claudia.binda@unipv.it, angelo.parini@inserm.fr, jeanne.perez@inserm.fr.

Running title : MAO-A and senescence

Key words: monoamine oxidase, senescence, oxidative stress, mitochondria, cardiac, mitophagy

For Peer Review

ScholarOne, 375 Greenbrier Drive, Charlottesville, VA, 22901 Support: (434) 964 4100

Summary

Cellular senescence, the irreversible cell-cycle arrest observed in somatic cells, is an important driver of age-dependent pathologies, including cardiac ageing. Mitochondria have been implicated in the process of cellular senescence, mostly due to the fact that they are both sources and targets of reactive oxygen species (ROS). Oxidative stress has been hypothesized to drive cardiac ageing and disease but the mechanisms underlying ROS production in the heart are still not completely understood. The mitochondrial enzyme monoamine oxidase-A (MAO-A) has been implicated in cardiac ageing possibly through the formation of hydrogen peroxide (H_2O_2) derived from the degradation of its substrates norepinephrine and serotonin. However, the potential link between MAO-A and senescence has never been investigated.

Using H9C2 cardiomyoblasts as a cellular model, we demonstrate that chronic MAO-A activation mediated by synthetic (Tyramine) and physiological (Norepinephrine) substrate, induces ROS-dependent DNA damage response (DDR), activation of Cyclin-Dependent Kinase Inhibitors p21, p16, p15, as well as increased cell size and SA-β-gal, typical of senescence. Moreover, we found that ROS produced by MAO-A induces accumulation of p53 to the cytosol where it inhibits Parkin, an important regulator of mitophagy, resulting in mitochondrial dysfunction. Importantly, activation of mitophagy, whether by overexpression of Parkin or mTOR inhibition, prevents mitochondrial dysfunction and as a result induction of senescence. Altogether, our data show a novel link between MAO-A and senescence in cardiac cells and provides mechanistic insights into the potential role of MAO-dependent oxidative stress in the development of age-related pathologies.

For Peer Review

ScholarOne, 375 Greenbrier Drive, Charlottesville, VA, 22901 Support: (434) 964 4100

Introduction

Cell senescence is a process by which stressed cells stop dividing, become resistant to apoptosis and undergo phenotypic remodelling with profound modification of their function and release of secretory factors (Childs, Durik, Baker, & van Deursen, 2015). Compelling evidence indicates that chronic accumulation of senescent cells with ageing is deleterious and participates in the functional decline of organs such as kidney, heart and liver (Baker et al., 2016; Zhu et al., 2015). One of the main characteristics of senescent cells is the activation of the DNA Damage Response (DDR) mechanism, which drives the expression of two major senescence pathways p53/$p21^{cip}$ and $p16^{ink4A}$, thereby maintaining retinoblastoma (Rb) in an active state to block cell cycle progression (Childs et al., 2015). Cell senescence has been classically considered as a result of telomere shortening. However, various experimental insults such as oxidative stress have been shown to induce a premature senescence named SIPS (Stress-Induced Premature Senescence), which may predispose individuals to age-related diseases (Giorgio, Trinei, Migliaccio, & Pelicci, 2007; Serrano & Blasco, 2001).

Mitochondria are both sources and targets of reactive oxygen species (ROS) and are considered as chief denominators of pathological ageing (Lopez-Otin, Blasco, Partridge, Serrano, & Kroemer, 2013). At the cellular level, converging evidences indicate that oxidative damage to mitochondria and cell senescence are interlinked processes (Ziegler, Wiley, & Velarde, 2015). This is well illustrated with the finding that complete removal of mitochondria prevents both replicative and stress-induced senescence in fibroblasts (Correia-Melo et al., 2016). It is believed that dysfunctional mitochondria may exacerbate ROS production and act as a feedback loop to stabilize DDR and senescence through the intervention of the mTOR/p70S6K kinase pathway (Correia-Melo et al., 2016; Nacarelli, Azar, & Sell, 2015). At present, the reason why damaged mitochondria accumulate with senescence is unclear, although it may involve increased biogenesis and/or disruption of mitophagy, a process that allows their elimination by the autophagy-lysosome pathway (Korolchuk, Miwa, Carroll, & von Zglinicki, 2017). In addition, there is still a strong need to ascertain the sources of mitochondrial ROS triggering SIPS, in order to identify new targets to retard age-associated disorders.

Monoamine oxidase-A (MAO-A) is a mitochondrial FAD-dependent enzyme that catalyses the oxidative deamination of serotonin and catecholamines to generate the corresponding aldehydes and hydrogen peroxide (H_2O_2) as byproducts. In the heart, MAO-A has been demonstrated to be a relevant source of oxidative stress in acute and chronic pathological situations (Bianchi et al., 2005; Kaludercic et al., 2010). In particular, cardiac overexpression of MAO-A drives oxidative stress and mitochondrial damage leading to cell death and heart failure (Kaludercic, Mialet-Perez, Paolocci, Parini, & Di Lisa, 2014; Villeneuve et al., 2013). Notably, all these effects are observed with high levels of MAO-A activation and H_2O_2 generation, and it is well known that depending on its concentration, H_2O_2 can produce dose-dependent cellular responses which range from proliferation to necrosis (Giorgio et al., 2007). p53 is one of the main effectors of the MAO-A/H_2O_2 axis (Villeneuve et al., 2013), which is at the crossroad of numerous signalling pathways and, depending on the extent of damage, can initiate DNA repair, senescence or cell death (Green & Kroemer, 2009). These observations, together with the fact that MAO-A expression increases in the ageing heart, led us to investigate whether a chronic increase in H_2O_2 through persistent MAO-A activation could potentially drive senescence in cardiac cells (Maurel et al., 2003).

Here, we demonstrate that MAO-driven ROS production at sub-lethal doses induces DDR and a senescence phenotype with increased expression of p21, p15 and p16, increased SA-β-gal activity and cell enlargement. Importantly, MAO-A activation leads to the accumulation of dysfunctional mitochondria through disruption of mitophagy, which is mediated by p53-induced Parkin inhibition. Moreover, we found that mTOR kinase pathway contributed to mitophagy dysfunction by enhancing p53 accumulation in the cytoplasm. Finally, inhibition of mitophagy and the resulting accumulation of damaged mitochondria were fully responsible for the persistence of the DDR network and the resolution of the senescence phenotype induced by MAO-A.

ScholarOne, 375 Greenbrier Drive, Charlottesville, VA, 22901 Support: (434) 964 4100

Results

MAO-A activity increases during ageing in isolated cardiomyocytes and triggers oxidative stress-mediated DNA damage response (DDR)

We first analyzed the effects of ageing on MAO expression, oxidative stress and senescent markers in mouse adult ventricular myocytes. MAO-A, but not MAO-B, was upregulated in 20 months-old compared to 3 months-old cardiomyocytes (Fig. 1A). This increase in MAO-A expression levels was paralleled by an increase in MAO-A enzymatic activity (Fig 1B). 4-hydroxynonenal (4-HNE) protein adducts, which are markers of oxidative stress, were significantly elevated in aged cardiomyocytes, together with p53, p21 and p15/p16 senescent markers (Fig. 1A, 1C). We next evaluated the putative causal link between enhanced MAO-A activity, ROS and senescent markers in H9C2 cells. We chose the substrate tyramine (Tyr), which is devoid of membrane receptors, in order to analyze only the effects due to MAO-A independently of receptor-mediated pathways. After 15 min of Tyr stimulation, we detected oxidation of the fluorescent probe DCFDA, which was completely prevented with the selective MAO-A inhibitor clorgyline (clorg), MAO-A knock-down with siRNA (siMAO-A) or the antioxidant Trolox (Fig. 1D and Suppl Fig. 1A). Among ROS, H_2O_2 is the main product resulting from the catalytic activity of MAO-A. H_2O_2 concentration was significantly elevated 1 h after Tyr stimulation, and prior application of clorg, Trolox or siMAO-A prevented this effect (Suppl. Fig. 1B). At the concentration used, Tyr incubated for 24 h was devoid of cytotoxic effects (Suppl. Fig. 1C, 1D, 1E). To evaluate whether MAO-A-induced oxidative stress led to DDR activation, the DNA damage was estimated over a 72 h period of Tyr stimulation. Comet assay showed a rapid and persistent increase in DNA strand-breaks from 6 h to 72 h after Tyr stimulation (Fig 1E). DDR is characterized by activation of ataxia-telangiectasia mutated kinase (ATM) and the formation of DNA-damage foci containing a phosphorylated form of H2A.X (γH2A.X). As expected, immunofluorescence assays revealed the presence of nuclear γH2A.X foci in cells stimulated with Tyr from 6 h to 72 h (Fig 1F). In line with these findings, an acute and persistent activation of DDR was confirmed by immunoblotting with a significant increase in the phosphorylation levels of ATM and H2A.X (Fig. 1G). Altogether, these observations demonstrate that chronic MAO-A activation at sub-lethal doses results in oxidative stress, DNA strand-breaks and persistent DDR.

MAO-A stimulation promotes Cyclin-Dependent Kinase Inhibitors (CDKi) activation and SIPS

Several studies have shown that the DDR is the main trigger of senescence, which leads to the downstream activation of CDKi of the p53/$p21^{cip}$ or the Ink4 family ($p15^{ink4b}$, $p16^{ink4A}$)(Campisi & d'Adda di Fagagna, 2007). These CDKi maintain the retinoblastoma protein (Rb) in a hypo-phosphorylated state, preventing the progression of the cell cycle. As shown in Fig. 2A, mRNA expression of the classical CDKi $p21^{cip}$, $p16^{ink4A}$ and $p15^{ink4b}$ was increased 72 h after Tyr treatment. In addition, we observed an increase in p53 phosphorylation (p-p53) at Ser15, an increase in total p53 and its downstream target p21, as well as a decrease in Rb phosphorylation (pRb) (Fig. 2B). Clorg and Trolox significantly prevented Tyr-induced p21 expression and Rb dephosphorylation, confirming the specific role of MAO-A in this pathway (Fig. 2C). Typical senescence phenotype is characterized by increased activity of β–galactosidase at pH 6, referred to as senescence-associated β–galactosidase (SA-β-gal). At 7 days post-Tyr exposure, cells showed increased frequency of SA-β-gal positive cells (Fig. 2D). In addition, cells became flattened and showed a significant increase in cell area (Fig. 2E). MAO-A inhibition with clorg and ROS scavenging totally prevented this senescent phenotype, as shown by a decrease in % positive SA-β-gal and decreased cell area (Fig. 2D, 2E). Finally, we measured the potential of the cell to proliferate 1 week after Tyr treatment. Proliferation rate was reduced with Tyr, compared to untreated cells and prior application of clorg and Trolox inhibited this effect (Suppl Fig. 1F).

Next, we evaluated whether the MAO-A/ROS/DDR/senescence pathway could be activated by the endogenous MAO substrate norepinephrine (NE), which is also known to exert many of its effects

ScholarOne, 375 Greenbrier Drive, Charlottesville, VA, 22901 Support: (434) 964 4100

through adrenergic receptors in cardiac cells. Application of 100 μM NE on H9C2 cells did not impair cell viability but increased oxidative stress, which was prevented by clorg, si-MAO-A and Trolox (Suppl Fig. 2A, 2B, 2C). As observed with Tyr, NE induced persistent activation of DDR over time, increase in mRNA levels of $p21^{cip}$, $p16^{ink4A}$ and $p15^{ink4b}$, increase in phospho(Ser15)-p53, p21 and decrease in pRB (Suppl. Fig. 2D, 2E, 2F). Clorg and Trolox reduced p21 and increased pRb expressions (Suppl. Fig. 2G). Finally, chronic treatment with NE (1 week) increased the frequency of SA-β-gal-positive cells and the average cell area, which were reduced by clorg and Trolox (Suppl. Fig. 3A-3B). The proliferation rate of the cells was decreased in the presence of NE, an effect that was significantly reduced with clorg and trolox (Suppl. Fig. 3C). Altogether, our findings demonstrate that MAO-A plays a significant role in the establishment of premature senescence induced by Tyr and NE.

MAO-A-induced cellular senescence is associated with mitochondrial dysfunction and inhibition of Parkin-mediated mitophagy

Accumulation of dysfunctional mitochondria seems to play a major role in stress-induced senescence. As MAO-A is bound to the mitochondrial outer membrane, we evaluated mitochondrial dynamics and function after cell treatment with Tyr for 72 h. The mitochondrial mass increased following Tyr stimulation, as shown with mitochondrial DNA copy number using mitoCytb and mitoNd1 (Fig. 3A). Since previous studies showed that increased mitochondrial biogenesis was part of the senescent phenotype, we measured the expression levels of its main transcriptional co-activators (Correia-Melo et al., 2016). mRNA analysis showed that PGC-1β expression was increased with Tyr, while PGC-1α was unchanged (Fig. 3B). A decrease in mitochondrial function, measured by the loss of mitochondrial membrane potential, was evidenced at 72 h (Fig. 3C). Furthermore, the levels of mtROS were increased, as shown by Mitosox staining (Suppl Fig. 4A) and mitochondrial 8-OH-dG staining which is indicative of mtDNA oxidation (Fig 3D). From these results, we infer that chronic MAO-A activation may result in the accumulation of damaged oxidized mitochondria. Mitochondrial integrity is maintained by the selective elimination of damaged mitochondria with engulfement into autophagosomes and degradation in the lysosomal compartment, a process termed mitophagy (Twig, Hyde, & Shirihai, 2008). Therefore, we investigated whether Tyr treatment led to any changes in mitophagy using immunofluorescence staining of the autophagosome marker EGFP-LC3 (green) and the mitochondrial marker MitoID (red). After 72 h of Tyr treatment, we could not detect any colocalization of mitochondria with the autophagosome marker LC3 (Fig. 3E). In addition, while treatment with CCCP (a well-known inducer of mitophagy) clearly induced colocalization of mitochondria with LC3 (yellow dots), Tyr reduced this induction of mitophagy by CCCP (Fig. 3E). To confirm these findings, we analyzed the subcellular localization of LC3II, p62 and ubiquitinated proteins in different conditions of stimulation. As expected, CCCP strongly induced the presence of LC3II, p62 and ubiquitinated proteins into mitochondrial fractions (Fig. 3F). However, Tyr alone failed to promote mitochondrial translocation of LC3 and p62. In addition, Tyr blocked the effects of CCCP on the accumulation of LC3II, p62 and ubiquitylated proteins in mitochondrial fractions (Fig. 3F). MAO-A -induced mitophagy inhibition was not due to a reduction of the total levels of LC3II and p62 (Suppl. Fig. 4B). One of the main mechanisms of clearance of damaged mitochondria involves the Pink1-Parkin-dependent pathway, which allows recruitment of the autophagosome machinery to the mitochondria (Vincow et al., 2013). Tyr treatment resulted in stabilization of Pink1 at the mitochondria, which is generally a consequence of a drop in mitochondrial membrane potential (Fig. 3G). Next, Pink1 allows the recruitment of the E3 ubiquitin ligase Parkin to mitochondria, promoting ubiquitination and targeting to autophagic vesicles. We observed that treatment with CCCP stimulated the translocation of Parkin from the cytoplasm to the mitochondria (Fig. 3H). However, Tyr failed to induce Parkin translocation in baseline conditions and prevented CCCP-induced translocation of Parkin to mitochondria (Fig. 3H). These effects were not due to a down-regulation of the total levels of Parkin with Tyr (Suppl. Fig. 4C). Therefore, chronic MAO-A stimulation inhibits Parkin translocation and

ScholarOne, 375 Greenbrier Drive, Charlottesville, VA, 22901 Support: (434) 964 4100

mitophagy, and thus may aggravate ROS-induced mitochondrial damage by preventing the clearance of oxidized mitochondria.

Mitophagy restoration prevents mitochondrial dysfunction and abolished MAO-A-induced senescent phenotype

Next, we overexpressed Parkin in cardiac cells to test whether mitophagy inhibition was interconnected with the activation of the senescence pathways. Transfected Parkin increased the total protein level of Parkin (Suppl Fig.5A) that was distributed both in cytoplasm and mitochondria (Fig. 4A, Suppl Fig.5B). Parkin overexpression restored mitophagy since its transfection was associated with enhanced mitochondrial expression of LC3II and p62 in both basal and Tyr-treated conditions (Fig. 4B). As expected, we observed an amelioration of mitochondrial dynamics and function in Parkin-transfected cells after Tyr treatment, as shown by decreased mitochondrial mass, preservation of mitochondrial membrane potential and inhibition of mitochondrial ROS compared with pcDNA3-transfected cells (Fig. 4C-E, Suppl. Fig. 5C). Next, we investigated the consequences of Parkin overexpression on the induction of senescence. Ectopic expression of Parkin did not influence the expression of γH2A.X at 6 h and 24 h after Tyr, but inhibited its long term persistence at 72 h (Fig. 4F). Consistenly, a strong decrease in p21 expression levels and SA-β-gal staining was observed in Parkin-transfected cells compared with pcDNA3-transfected cells after Tyr stimulation (Fig 4G, 4H). This effect was not due to a decrease in MAO-A expression (Suppl. Fig. 5D). Our data suggest that chronic oxidative stress and maintenance of the DDR are dependent on mitophagy impairment and mitochondrial dysfunction, which strongly impact on MAO-A-induced cell senescence.

Crosstalk between p53 and mTOR pathways regulate mitochondrial dysfunction-associated senescence induced by MAO-A

Next we investigated how mitochondrial Parkin translocation was impaired during Tyr treatment. It is known that Parkin translocation can be inhibited by interaction with cytosolic p53 (Hoshino et al., 2013). In H9C2 cells, Tyr treatment for 72 h induced accumulation of cytosolic p53 levels and increased p53-Parkin interaction (Fig. 5A, 5B). Interestingly, siRNA p53-transfected cells (Fig. 5C) showed higher levels of mitochondrial Parkin than siRNA-Scr-transfected cells in Tyr treated cells (Fig. 5D). Yet, mitochondrial levels of LC3II and p62 were strongly increased by Tyr, indicative of enhanced mitophagy when p53 was silenced (Fig. 5E). These results suggest that the accumulation of p53 impairs Parkin-mediated mitophagy in senescent cells.

Another major regulator of mitochondrial homeostasis and senescence is the protein kinase mTOR, which has been demonstrated to regulate p53 accumulation through MDM2-dependent or independent mechanisms (Lai et al., 2010). In cells stimulated with Tyr, mTOR was persistently activated, as shown by the phosphorylation level of its major target p70S6K, and this was prevented with the mTOR inhibitor rapamycin (Fig. 5F). Since rapamycin treatment inhibited Tyr-induced p53 accumulation in the cytosol (Fig. 5G), we thus evaluated if mTOR inhibition translated into an amelioration of mitophagy. As shown in Fig. 6A-6B, inhibition of mTOR with rapamycin restored the translocation of Parkin at the mitochondria in the presence of Tyr and stimulated mitophagy, as shown by the mitochondrial accumulation of LC3II and p62 (Fig. 6A, 6B and Suppl. Fig. 6A). As a consequence of amelioration of mitophagy, rapamycin also prevents various Tyr-induced mitochondrial dysfunction (Fig. 6C-6E, Suppl Fig. 6B). The levels of pH2A.X were decreased at 72 h of Tyr treatment in the presence of rapamycin, compared to vehicle-treated cells (Fig. 6F) and p21 and SA-β-Gal were inhibited (Fig. 6G-6H). Altogether, these data show that mTOR is a master regulator of p53-parkin mitophagy and senescence.

For Peer Review

ScholarOne, 375 Greenbrier Drive, Charlottesville, VA, 22901 Support: (434) 964 4100

Discussion

This study shows for the first time that MAO-A can drive SIPS in cardiac cells through ROS production and mitochondrial dysfunction.

MAO-A-driven H_2O_2 production has been previously assigned to different types of cellular responses such as hypertrophy and death (Kaludercic et al., 2014) . In addition, elevated MAO-A expression in prostate cancer cells was recently shown to promote metastasis by two distinct mechanisms such as epithelial-to-mesenchymal transition and paracrine Shh signaling (Wu et al., 2014; Wu et al., 2017). These particular responses might depend on the cell type, but also on the amount of H_2O_2, which is known to drive dose-dependent cellular effects (Duan, Duan, Zhang, & Tong, 2005; Giorgio et al., 2007). During cardiac ischemia-reperfusion injury, where high levels of MAO substrates are released as well as in the hearts of transgenic mice overexpressing MAO-A, cell apoptosis and necrosis are preferentially activated together with lysosomal alteration-induced blockade of the autophagic flux (Bianchi et al., 2005; Santin et al., 2016; Villeneuve et al., 2013). Here, we demonstrate that chronic sub-lethal doses of H_2O_2 produced by MAO-A in response to its endogenous (NE) or exogenous (Tyr) substrates can recapitulate all the features of senescence. This could have particular relevance in cardiac ageing, where MAO-A is likely to be chronically activated due to: i) sympathetic activation and enhanced release of norepinephrine from adrenergic nerves (Santulli & Iaccarino, 2016); ii) overexpression of MAO-A in the ageing heart (as shown in Fig. 1A, 1B) or in age-associated cardiac diseases (Manni et al., 2016; Villeneuve et al., 2013). In addition, the role of MAO-A in senescence could be extended to different cell types since MAO-A has been characterized in many proliferative cells such as fibroblasts and bone marrow mesenchymal stem cells, where its expression was significantly increased during ageing, (Edelstein & Breakefield, 1986; Trouche et al., 2010).

Cell senescence and mitochondrial dysfunction are considered as essential “hallmarks of ageing” and our data provide additional evidence that they are closely interlinked (Lopez-Otin et al., 2013). Indeed, we observed that mitochondrial dysfunction was necessary for the establishment of the senescent phenotype in response to chronic MAO-A stimulation. Restauration of mitochondrial clearance with parkin prevented persistence of the DDR and establishment of senescence. Indeed, in our model, maintenance of the DDR is tightly controlled by the mitochondria through an amplification loop involving ROS. Parkin overexpression inhibited mitochondrial ROS accumulation (Mitosox red) and mitochondrial DNA oxidation (8-OH-dG), the latter being strongly associated with the ageing process (Barja & Herrero, 2000). Thus, mitochondrial dysfunction through ROS accumulation likely contributes to DDR establishment and senescence. In a previous study, Correia-Melo et al. reported that mitochondria were necessary for replicative and irradiation-induced premature senescence in fibroblasts (Correia-Melo et al., 2016). In this case, they also observed mitochondrial ROS accumulation and increased mitochondrial mass, but the main drivers of senescence were mitochondrial biogenesis and PGC-1β activation. This is different from the present study where we show that accumulation of mitochondria is mostly due to the inhibition of mitophagy. However, we cannot exclude a participation of mitochondrial biogenesis as we showed enhanced levels of PGC-1β mRNA after MAO-A activation with Tyr. It is possible that enhanced biogenesis in a situation of mitophagy blockade increases the burden of mitochondrial damage, further contributing to ROS-DDR and senescence.

While we found that mitochondrial dysfunction participated in DDR maintenance, on turn, it is also possible that DDR maintains mitochondrial dysfunction. Our main results showed that p53, which was under the regulation of the DDR pathway, inhibited mitophagy through its direct interaction with Parkin in the cytosol. Releasing this inhibition by p53 knock-down prevented the decrease in mitochondrial membrane potential and inhibited mitochondrial ROS accumulation. Our results are consistent with previous studies showing that p53-Parkin inhibition pathway plays an important role in cardiac ageing and drives age-related diseases such as heart failure and diabetes (Hoshino et al., 2014; Hoshino et al., 2013). Notably, we provide additional evidence that p53 is a major mediator of MAO-A-dependent

ScholarOne, 375 Greenbrier Drive, Charlottesville, VA, 22901 Support: (434) 964 4100

response. Being at the hub of many signalling pathways, we believe that, depending on different stress conditions, p53 can mediate either MAO-A/H_2O_2-dependent senescence or cell death, as already demonstrated for other stress-driven mechanisms (Green & Kroemer, 2009).

Looking for regulatory pathways able to regulate mitochondrial homeostasis, we observed that the mTORC1 kinase complex was potently activated in Tyr-stimulated cells. There have been many reports of aberrant activation of mTOR during ageing and inhibition of mTOR pathway seems to be the most convincing intervention to prolong lifespan and retard age-associated disorders. mTOR can be activated by the DDR through the ATM-Akt signalling (Correia-Melo et al., 2016). In the present study, we did not evaluate this possibility, knowing that mTOR can also be activated by many distinct pathways, or directly by ROS (Sarbassov & Sabatini, 2005). We thus tried to understand the consequences of mTOR activation on mitochondrial homeostasis. The mTORC1 complex is well known to inhibit global autophagy through phosphorylation of the initiation complex ULK1 (Nacarelli et al., 2015). However, global autophagy was not modified after MAO-A stimulation, with no differences in LC3II or p62 levels. Indeed, the regulation of the autophagic machinery during senescence is contradictory, some studies showing higher levels and other showing lower levels. Conversely, a substantial impairment of mitophagy was consistently observed (Korolchuk et al., 2017). While mTOR has been clearly involved in the regulation of mitochondrial homeostasis and mitochondrial biogenesis (Morita et al., 2013), the possibility that it regulates mitophagy has been underestimated. Here, we provide evidence that rapamycin, an inhibitor of the mTORC1 complex, completely restores mitophagy and prevents all the features associated with mitochondrial dysfunction, DDR and senescence. In addition, we describe for the first time the interaction between two major senescence-associated pathways, mTOR and p53, which cooperate to inhibit mitophagy and stabilize DDR and senescence in response to MAO-A (Suppl. Fig. 7) (Nacarelli et al., 2015).

Finally, it is possible that MAO-A-driven SIPS may act as a deleterious mechanism, enhancing the susceptibility of the elderly to cardiac diseases. This will need to be evaluated in future studies, together with the possibility that MAO-A inhibition may prevent or reduce cardiac pathological ageing.

Experimental procedures

Materials

Tyramine, norepinephrine, clorgyline, trolox, rapamycin were from Sigma-Aldrich (St. Louis, MO, USA). The 3X-HA-3X-Flag-hparkin insert was subcloned from pcDNA5/FRT/TO into pcDNA3 plasmid (pcDNA5/FRT/TO was a generous gift from Lars Dreir, Department of Neurobiology at UCLA, Los Angeles, USA) to. The pEGFP-LC3 plasmid was from Adgene.

Cell culture

Adult ventricular myocytes were obtained from hearts of male C57Bl6J mice at 3 and 20 months as previously described (Fazal et al., 2017). Rat H9c2 cardiomyoblasts (American Type Culture Collection, Rockville, U.S.A.) were grown in DMEM media containing 10% heat-inactivated FBS under 5% CO2 and 95% air at 37°C. H9C2 serves as an animal-free alternative sharing many physiological properties of primary cardiac cells (Watkins, Borthwick, & Arthur, 2011). Cells were transfected with MAO-A siRNA, p53 siRNA or scramble siRNA (On-target-plus smart pool, Dharmacon) with DharmaFECT Duo (Dharmacon). Plasmid transfections were performed with Lipofectamine (Thermo Fisher scientific).

Subcellular fractioning and Western blot analysis

Mitochondrial and cytosolic fractions were isolated using a commercial kit (Quiagen, Germany). For whole-cell lysates, cells were collected in RIPA buffer (20 mMTris-HCl, 150 mM NaCl, 1 mM EDTA, 1% NP40, 0.1% SDS, antiphosphates and antiproteases) and centrifuged at 13,000 g for 5 min to keep the supernatant. Equal amount of proteins were electrophoresed and transferred to a nitrocellulose

ScholarOne, 375 Greenbrier Drive, Charlottesville, VA, 22901 Support: (434) 964 4100

membrane. Primary antibody incubations were performed with anti-MAO-A or anti-Parkin from Abcam; anti-p53, anti-phospho-p53(ser15), anti-H2A.X, anti-Pink1, anti-LC3, anti-Ubiquitin, anti-phospho-Rb(Ser807/811), anti-phospho-p70S6K(Thr389) from Cell Signaling Technologies; anti-phospho-H2A.X(Ser139) from Millipore; anti-p62 from Abnova; anti-ATM, anti-phospho-ATM(Ser1981), anti-p21 from Santa-Cruz Biotechnology. Images were taken with the ChemiDoc-MP Imaging System and quantified using Image-Lab 4.0 software (Bio-Rad).

Immunoprecipitation assay

For immunoprecipitation (IP), cytosolic fractions were incubated with anti-p53 or anti-Parkin antibodies for 12 h at 4°C. Protein A/G Plus-Agarose was then added for 3 h at 4°C on a rotating device. Immunoprecipitates were collected by centrifugation at 6000 g at 4 °C and washed with lysis buffer (20mM Tris pH 7.5, 150 mM NaCl, 1 mM EDTA, 1% Triton X100, proteases and phosphatases inhibitors). The pellets were eluted by heating at 95°C for 5 min in electrophoresis sample buffer and subjected to immunoblotting.

Immunofluorescence

H9c2 cells were fixed with PFA 4%, permeabilized with Triton 0.5 %, blocked with BSA 3 % and incubated with anti-Vinculin (Sigma) or Anti-pH2A.X (Millipore) overnight at 4°C. Secondary antibody was Alexa-Green-488 goat anti-mouse (Invitrogen). Images were acquired using epifluorescence microscopy (DM600 microscope, Leica). For mitophagy detection, EGFP-LC3 plasmid and MitoID (Enzo) were used to stain autophagosomes and mitochondria, respectively. Image acquisition was performed with a LSM780 laser scanning confocal (Carl Zeiss). For mitochondrial 8-OH-dG detection, cells were fixed with methanol for 30 min at -20°C, permeabilized with 0.2% Triton and treated with Rnase A at 37° C for 1h, followed by denaturation with ice-cold 25 mM NaOH in 50 % ethanol as previously described (Ohno, Oka, & Nakabeppu, 2009). After blocking with BSA 10%, cells were incubated with mouse anti-8-OH-dG (clone 483.15, Millipore) overnight at 4°C. Secondary antibody was goat anti-mouse Alexa 488.

Comet assay

DNA breaks were measured with the Comet assay, as previously described (Collins et al., 2008). Cell suspension was mixed with 1% low melting point agarose, and the mixture was spread onto slides precoated with 1% of normal melting point agarose (Sigma). Glass cover slips were placed on the drops of agarose, which were allowed to set at 4 °C. Then, the cover slips were removed and the cells embedded in agarose were lysed for 1 h by immersion in lysis solution (2.5 M NaCl, 0.1 M Na2EDTA, 0.1 M Tris base, pH 10 and 1% Triton X-100) at 4 °C. The slides were then placed in a horizontal gel electrophoresis tank and the DNA was allowed to unwind for 40 min in freshly prepared alkaline electrophoresis solution (0.3 M NaOH and 1 mM Na2EDTA, pH > 13). Electrophoresis was carried out in the alkaline solution for 30 min at 4 °C. The slides were washed in 0.4 M Tris base (pH 7.5) for 10 min at 4 °C to neutralize the excess alkali and 10 min in water at 4 °C. Then they were left to dry overnight. Gels were stained with 25 µL of DAPI, covered with a cover slip and coded before microscopic analysis. DAPI-stained nuclei were evaluated with a fluorescence microscope

Total ROS

Cellular ROS were measured using the fluorescent probe DCFDA assay at a concentration of 5 µM (ThermoFisher Scientific).

SA-β-gal staining

SA-β-Gal activity was measured as previously described (Duan et al., 2005). Cells fixed in PFA were stained with SA-β-Gal stain solution (1mg/ml X-gal, 40mM citric acid/sodium phosphate, pH 6, 5mM

ScholarOne, 375 Greenbrier Drive, Charlottesville, VA, 22901 Support: (434) 964 4100

potassium ferrocyanide, 5mM potassium ferricyanide, 150 mM NaCl, 2mM $MgCl_2$). After 16 hours at 37°C, images were taken using a brightfield microscope.

JC1 staining

The mitochondrial membrane potential was evaluated by JC1 probe (ThermoFisher Scientific). Before the end of treatments, cells were loaded with JC1 probe at a concentration of 5 µg/ml for 15 min and analyzed for imaging at confocal microscope.

Real-time RT-PCR

Extraction of RNA from H9c2 cells was performed using column affinity purification (Qiagen). cDNAs were synthesized using the iScript RT master mix (Bio-Rad) with random hexamers. Real-time PCR was performed on a StepOnePlus system (Applied Biosystem) in 96-well plates with specific primers and SYBR green mix (Biorad). Rat primers were as followed: PGC-1α-F: CACCAAACCCACAGAGAACAG, PGC-1α-R: GCAGTTCCAGAGAGTTCCACA; PGC1-β-F: TTGTGTCAAGGTGGATGGCA and PGC-1β-R: GCACCGAAGTGAGGTGCTTA; p21-F: TGCCGAAGTCAGTTCCTTGT and p21-R: GTTCTGACATGGCGCCTCC; p16-F: CTTCGGCTGACTGGCTGG and p16-R: TCATCATGACCTGGATCGGC; p15-F: GGGACTAGTGGAGAAGGTGC and p15-R: CATCATCATGACCTGGATCGC; GAPDH-F: TCTCTGCTCCTCCCTGTTCTA; GAPDH-R: TCCGATACGGCCAAATCCGTT was used as endogenous control. The relative mRNA expression levels were calculated applying the following equation: $2^{-\Delta Ct}$, and the fold change value of expression compared to a control was calculated following the ΔΔCt method.

mtDNA copy number

mtDNA copy number was evaluated by Real-Time PCR on extracted DNA with specific primers for mitochondrial (ND1-F: ATGGATTCGAGCATCCTACCC, ND1-R: TCCTGCTAGGAAAATTGGCA; CytB-F: TGCCGAGACGTAAACTACGG, CytB-R: TAGTCCTCGTCCCACATGGA) and nuclear gene (β-actin-F: GCAGGAGTACGATGAGTCCG, β-actin-R: ACGCAGCTCAGTAACAGTCC). The mtDNA copy number was normalized to nuclear gene.

Statistical analysis

Statistical analysis was calculated using student t-test or 2-way ANOVA with Tukey post-hoc test, when appropriate. The results were shown as the means ± SEM. Values of $p<0.05$ were considered significant.

Acknowledgment

This work was supported by grants from Agence Nationale pour la Recherche (ANR jcjc “CardioMAO”), Fondation pour la Recherche Médicale (“Equipes FRM 2016”, DEQ20160334892), Fondazione Cariplo (grant 2014-0672) and Région Occitanie.

Author contributions

NM designed, performed and analyzed the majority of experiments. DM, YS and HM performed and analyzed individual experiments. VDE, CB and JMP designed and supervised individual experiments. FL, CB, AP, JFP and JMP supervised the study and wrote the manuscript with contributions from all authors.

References

Baker, D. J., Childs, B. G., Durik, M., Wijers, M. E., Sieben, C. J., Zhong, J., . . . van Deursen, J. M. (2016). Naturally occurring p16(Ink4a)-positive cells shorten healthy lifespan. *Nature, 530*(7589), 184-189. doi: 10.1038/nature16932

ScholarOne, 375 Greenbrier Drive, Charlottesville, VA, 22901 Support: (434) 964 4100

For Peer Review

Barja, G., & Herrero, A. (2000). Oxidative damage to mitochondrial DNA is inversely related to maximum life span in the heart and brain of mammals. *Faseb J, 14*(2), 312-318.

Bianchi, P., Kunduzova, O., Masini, E., Cambon, C., Bani, D., Raimondi, L., . . . Parini, A. (2005). Oxidative stress by monoamine oxidase mediates receptor-independent cardiomyocyte apoptosis by serotonin and postischemic myocardial injury. *Circulation, 112*(21), 3297-3305.

Campisi, J., & d'Adda di Fagagna, F. (2007). Cellular senescence: when bad things happen to good cells. *Nat Rev Mol Cell Biol, 8*(9), 729-740. doi: 10.1038/nrm2233

Childs, B. G., Durik, M., Baker, D. J., & van Deursen, J. M. (2015). Cellular senescence in aging and age-related disease: from mechanisms to therapy. *Nature Medicine, 21*(12), 1424-1435. doi: 10.1038/nm.4000

Collins, A. R., Oscoz, A. A., Brunborg, G., Gaivao, I., Giovannelli, L., Kruszewski, M., . . . Stetina, R. (2008). The comet assay: topical issues. *Mutagenesis, 23*(3), 143-151. doi: 10.1093/mutage/gem051

Correia-Melo, C., Marques, F. D., Anderson, R., Hewitt, G., Hewitt, R., Cole, J., . . . Passos, J. F. (2016). Mitochondria are required for pro-ageing features of the senescent phenotype. *EMBO J, 35*(7), 724-742. doi: 10.15252/embj.201592862

Duan, J., Duan, J., Zhang, Z., & Tong, T. (2005). Irreversible cellular senescence induced by prolonged exposure to H2O2 involves DNA-damage-and-repair genes and telomere shortening. *Int J Biochem Cell Biol, 37*(7), 1407-1420. doi: 10.1016/j.biocel.2005.01.010

Edelstein, S. B., & Breakefield, X. O. (1986). Monoamine oxidases A and B are differentially regulated by glucocorticoids and "aging" in human skin fibroblasts. *Cell Mol Neurobiol, 6*(2), 121-150.

Fazal, L., Laudette, M., Paula-Gomes, S., Pons, S., Conte, C., Tortosa, F., . . . Lezoualc'h, F. (2017). Multifunctional Mitochondrial Epac1 Controls Myocardial Cell Death. *Circ Res, 120*(4), 645-657. doi: 10.1161/CIRCRESAHA.116.309859

Giorgio, M., Trinei, M., Migliaccio, E., & Pelicci, P. G. (2007). Hydrogen peroxide: a metabolic by-product or a common mediator of ageing signals? *Nat Rev Mol Cell Biol, 8*(9), 722-728.

Green, D. R., & Kroemer, G. (2009). Cytoplasmic functions of the tumour suppressor p53. *Nature, 458*(7242), 1127-1130. doi: 10.1038/nature07986

Hoshino, A., Ariyoshi, M., Okawa, Y., Kaimoto, S., Uchihashi, M., Fukai, K., . . . Matoba, S. (2014). Inhibition of p53 preserves Parkin-mediated mitophagy and pancreatic beta-cell function in diabetes. *Proc Natl Acad Sci U S A, 111*(8), 3116-3121. doi: 10.1073/pnas.1318951111

Hoshino, A., Mita, Y., Okawa, Y., Ariyoshi, M., Iwai-Kanai, E., Ueyama, T., . . . Matoba, S. (2013). Cytosolic p53 inhibits Parkin-mediated mitophagy and promotes mitochondrial dysfunction in the mouse heart. *Nat Commun, 4*, 2308. doi: 10.1038/ncomms3308

Kaludercic, N., Mialet-Perez, J., Paolocci, N., Parini, A., & Di Lisa, F. (2014). Monoamine oxidases as sources of oxidants in the heart. *J Mol Cell Cardiol, 73*, 34-42. doi: 10.1016/j.yjmcc.2013.12.032

Kaludercic, N., Takimoto, E., Nagayama, T., Feng, N., Lai, E. W., Bedja, D., . . . Paolocci, N. (2010). Monoamine oxidase A-mediated enhanced catabolism of norepinephrine contributes to adverse remodeling and pump failure in hearts with pressure overload. *Circ Res, 106*(1), 193-202.

Korolchuk, V. I., Miwa, S., Carroll, B., & von Zglinicki, T. (2017). Mitochondria in cell senescence: Is mitophagy the weakest link? *EBioMedicine*. doi: 10.1016/j.ebiom.2017.03.020

Lai, K. P., Leong, W. F., Chau, J. F., Jia, D., Zeng, L., Liu, H., . . . Li, B. (2010). S6K1 is a multifaceted regulator of Mdm2 that connects nutrient status and DNA damage response. *EMBO J, 29*(17), 2994-3006. doi: 10.1038/emboj.2010.166

Lopez-Otin, C., Blasco, M. A., Partridge, L., Serrano, M., & Kroemer, G. (2013). The hallmarks of aging. *Cell, 153*(6), 1194-1217. doi: 10.1016/j.cell.2013.05.039

Manni, M. E., Rigacci, S., Borchi, E., Bargelli, V., Miceli, C., Giordano, C., . . . Nediani, C. (2016). Monoamine Oxidase Is Overactivated in Left and Right Ventricles from Ischemic Hearts: An

ScholarOne, 375 Greenbrier Drive, Charlottesville, VA, 22901 Support: (434) 964 4100

Intriguing Therapeutic Target. *Oxid Med Cell Longev, 2016*, 4375418. doi: 10.1155/2016/4375418

Maurel, A., Hernandez, C., Kunduzova, O., Bompart, G., Cambon, C., Parini, A., & Frances, B. (2003). Age-dependent increase in hydrogen peroxide production by cardiac monoamine oxidase A in rats. *Am J Physiol Heart Circ Physiol, 284*(4), H1460-1467.

Morita, M., Gravel, S. P., Chenard, V., Sikstrom, K., Zheng, L., Alain, T., . . . Sonenberg, N. (2013). mTORC1 controls mitochondrial activity and biogenesis through 4E-BP-dependent translational regulation. *Cell Metab, 18*(5), 698-711. doi: 10.1016/j.cmet.2013.10.001

Nacarelli, T., Azar, A., & Sell, C. (2015). Aberrant mTOR activation in senescence and aging: A mitochondrial stress response? *Exp Gerontol, 68*, 66-70. doi: 10.1016/j.exger.2014.11.004

Ohno, M., Oka, S., & Nakabeppu, Y. (2009). Quantitative analysis of oxidized guanine, 8-oxoguanine, in mitochondrial DNA by immunofluorescence method. *Methods Mol Biol, 554*, 199-212. doi: 10.1007/978-1-59745-521-3_13

Santin, Y., Sicard, P., Vigneron, F., Guilbeau-Frugier, C., Dutaur, M., Lairez, O., . . . Mialet-Perez, J. (2016). Oxidative Stress by Monoamine Oxidase-A Impairs Transcription Factor EB Activation and Autophagosome Clearance, Leading to Cardiomyocyte Necrosis and Heart Failure. *Antioxid Redox Signal, 25*(1), 10-27. doi: 10.1089/ars.2015.6522

Santulli, G., & Iaccarino, G. (2016). Adrenergic signaling in heart failure and cardiovascular aging. *Maturitas, 93*, 65-72. doi: 10.1016/j.maturitas.2016.03.022

Sarbassov, D. D., & Sabatini, D. M. (2005). Redox regulation of the nutrient-sensitive raptor-mTOR pathway and complex. *J Biol Chem, 280*(47), 39505-39509. doi: 10.1074/jbc.M506096200

Serrano, M., & Blasco, M. A. (2001). Putting the stress on senescence. *Curr Opin Cell Biol, 13*(6), 748-753.

Trouche, E., Mias, C., Seguelas, M. H., Ordener, C., Cussac, D., & Parini, A. (2010). Characterization of monoamine oxidases in mesenchymal stem cells: role in hydrogen peroxide generation and serotonin-dependent apoptosis. *Stem Cells Dev, 19*(10), 1571-1578. doi: 10.1089/scd.2009.0353

Twig, G., Hyde, B., & Shirihai, O. S. (2008). Mitochondrial fusion, fission and autophagy as a quality control axis: the bioenergetic view. *Biochim Biophys Acta, 1777*(9), 1092-1097. doi: 10.1016/j.bbabio.2008.05.001

Villeneuve, C., Guilbeau-Frugier, C., Sicard, P., Lairez, O., Ordener, C., Duparc, T., . . . Mialet-Perez, J. (2013). p53-PGC-1alpha pathway mediates oxidative mitochondrial damage and cardiomyocyte necrosis induced by monoamine oxidase-A upregulation: role in chronic left ventricular dysfunction in mice. *Antioxid Redox Signal, 18*(1), 5-18. doi: 10.1089/ars.2011.4373

Vincow, E. S., Merrihew, G., Thomas, R. E., Shulman, N. J., Beyer, R. P., MacCoss, M. J., & Pallanck, L. J. (2013). The PINK1-Parkin pathway promotes both mitophagy and selective respiratory chain turnover in vivo. *Proc Natl Acad Sci U S A, 110*(16), 6400-6405. doi: 10.1073/pnas.1221132110

Watkins, S. J., Borthwick, G. M., & Arthur, H. M. (2011). The H9C2 cell line and primary neonatal cardiomyocyte cells show similar hypertrophic responses in vitro. *In Vitro Cell Dev Biol Anim, 47*(2), 125-131. doi: 10.1007/s11626-010-9368-1

Wu, J. B., Shao, C., Li, X., Li, Q., Hu, P., Shi, C., . . . Chung, L. W. (2014). Monoamine oxidase A mediates prostate tumorigenesis and cancer metastasis. *J Clin Invest, 124*(7), 2891-2908. doi: 10.1172/JCI70982

Wu, J. B., Yin, L., Shi, C., Li, Q., Duan, P., Huang, J. M., . . . Chung, L. W. (2017). MAOA-Dependent Activation of Shh-IL6-RANKL Signaling Network Promotes Prostate Cancer Metastasis by Engaging Tumor-Stromal Cell Interactions. *Cancer Cell, 31*(3), 368-382. doi: 10.1016/j.ccell.2017.02.003

Zhu, Y., Tchkonia, T., Pirtskhalava, T., Gower, A. C., Ding, H., Giorgadze, N., . . . Kirkland, J. L. (2015). The Achilles' heel of senescent cells: from transcriptome to senolytic drugs. *Aging Cell, 14*(4), 644-658. doi: 10.1111/acel.12344

ScholarOne, 375 Greenbrier Drive, Charlottesville, VA, 22901 Support: (434) 964 4100

Ziegler, D. V., Wiley, C. D., & Velarde, M. C. (2015). Mitochondrial effectors of cellular senescence: beyond the free radical theory of aging. *Aging Cell, 14*(1), 1-7. doi: 10.1111/acel.12287

Figure Legends

Fig 1. Monoamine oxidase-A (MAO-A) and oxidative stress are increased in senescent mouse cardiomyocytes and stimulation of MAO-A triggers ROS-dependent DNA damage response in H9C2 cells (A) Immunoblots of MAO-A, MAO-B and 4-HNE protein adducts in adult ventricular myocytes from young (3 months) and old mice (20 months). Quantifications of the ratios to GAPDH are shown in the lower panel (N=4). **(B)** MAO-A activity in isolated cardiomyocytes from young (3 months) and old mice (20 months) (N=4). **(C**) Immunoblots of p53, p21 and p15/p16 proteins in adult ventricular myocytes from young (3 months) and old mice (20 months) Quantifications of the ratios to GAPDH are shown in the lower panel (N=4). **(D)** DCFDA oxidation in response to 500 μM Tyr for 15 min, and in the presence of clorg (10 µ*M*), siMAO-A siRNA or Trolox (500 µM), when indicated (N=3). **(E)** Comet Assay representing DNA damage (DNA Strand Breaks) in cells treated with Tyr (500 µM*)* for the indicated time. Scale Bar = 10µm. Images are representative of N=3 experiments. **(F)** DNA damage foci (reflected by γH2A.X foci) in cells treated with 500 µ*M* Tyr for the indicated times. DAPI (blue) was used to label nucleus and γ-H2A.X for DNA damage foci (green). Scale Bar = 10µm. Images are representative of N=3 experiments**. (G)** Immunoblots of total and phosphorylated levels of H2A.X and ATM in cell extracts after stimulation with Tyr (500 µ*M*) for the indicated time. Actin was used as loading control. Quantifications of the ratios of phospho-H2A.X on total H2A.X and phospho-ATM on total ATM are shown in the lower panels (N=3). Data are expressed as means ± sem (**p*<0.05, ***p*<0.01, ***p<0.001 vs young mice or control; §*p*<0.05, §§*p*<0.01, §§§p<0.001 vs Tyr).

Fig.2. MAO-A activation induces expression of cell cycle inhibitors and senescence markers. (A) Analysis of mRNA levels of CDKi p21, p16 and p15 normalized to GAPDH by real-time RT-PCR in cells stimulated with 500 µM Tyr for 72 h (N=5). **(B)** Immunoblots of phosphoSer15-p53, total p53, p21 and pRb in cells stimulated with 500 µM Tyr for the indicated times. Quantifications of the ratios to actin are shown on the histograms (right panel) (N=3). **(C)** Immunoblots of p21 and pRb in cells stimulated with 500 µM Tyr for 72 h in control conditions or in the presence of clorg (10 µ*M*) or Trolox (500 µM), when indicated. Quantifications of the ratios to actin are shown on the histograms below (N=3). **(D)** Representative images and quantitative analysis of SA-β-gal activity in cells stimulated with 500 µM Tyr for 1 week in the presence of clorg (10 µM) or Trolox (500 µM), when indicated. The number of blue cells was counted and expressed as percent of total cell number. For each condition, a total of 100 cells were counted (N=4). **(E)** Representative images and quantitative analysis of cell area after stimulation with 500 µM Tyr for 1 week in the presence of clorg (10 µM) or Trolox (500 µM), when indicated. DAPI (blue) was used to label nucleus and Vinculin for cell size measurement (green). Scale Bar= 10µm. For each condition, a total of 100 cells were counted (N=4). Data are expressed as means ± sem (**p*<0.05, ***p*<0.01, *** p<0.001 vs control; §*p*<0.05, §§*p*<0.01, §§§p<0.001 vs Tyr).

Fig. 3. MAO-A activation induces mitochondrial dysfunction and mitophagy impairment. (A) mtDNA copy number analysis (Nd1/Actin and Cytb/Actin) by real-time PCR in H9C2 treated with 500 µ*M* Tyr for 72 h (N=5). **(B)** Analysis of mRNA levels of PGC-1α and pGC-1β normalized to GAPDH by real-time RT-PCR in cells stimulated with 500 µM Tyr for 72 h (N=3). **(C)** Quantitative analysis and representative picture of mitochondrial membrane potential with JC1 staining in H9C2 treated with 500 µM Tyr for 72 h (N=8). **(D)** Representative picture of mitochondrial 8-OH-dG immunostaining in H9C2 treated with 500 µM Tyr for 72 h (N=3). **(E)** Representative confocal images of LC3-EGFP-transfected cells stained with MitoID Red. Cells were treated with 500 µM Tyr for 72 h, followed by 50 µ*M* CCCP treatment for 6 h,

ScholarOne, 375 Greenbrier Drive, Charlottesville, VA, 22901 Support: (434) 964 4100

when indicated (N=3). **(F)** Analysis of LC3, p62 and ubiquitylated proteins in mitochondrial extracts of H9C2 stimulated with 500 µM Tyr for 72 h followed by 50 µ*M* CCCP, when indicated. VDAC was used as a loading control for mitochondrial proteins (N=3). **(G)** Analysis of PINK1 by immunoblot in mitochondrial extracts of H9c2 stimulated with 500 µM Tyr for 72 h. VDAC was used as a loading control (N=3). **(H)** Analysis of Parkin by immunoblot in cytosolic and mitochondrial extracts of H9C2 cells stimulated with 500 µM Tyr for 72 h followed by 50 µ*M* CCCP treatment for 6 h, when indicated; GAPDH and VDAC were used as loading controls for cytosolic and mitochondrial fractions, respectively (N=4). Data are expressed as means ± sem (**p*<0.05, ***p*<0.01, ***p<0.001 vs control).

Fig. 4. Restauration of Parkin-mediated mitophagy prevents induction of senescence. H9C2 cells were transfected with pcDNA3 or Parkin and stimulated with 500 µM Tyr for 72 h. **(A)** Analysis of Parkin by immunoblot in cytosolic and mitochondrial extracts. GAPDH and VDAC are used as loading controls for cyto and mito fractions, respectively (N=3). **(B)** Analysis of LC3 and p62 in mitochondrial extracts. VDAC was used as a loading control (N=3). **(C)** mtDNA copy number (Nd1/Actin) by real-time PCR (N=3). **(D)** Quantitative analysis of mitochondrial membrane potential with JC1 probe (N=3). **(E)** Representative images of mitochondrial 8-OH-dG immunostaining (N=3). **(F)** Analysis of total and pH2A.X by immunoblotin cells stimulated with Tyr for the indicated times. Actin was used as a loading control (N=3). **(G)** Analysis of p21 expression. Actin was used as a loading control (N=3). **(H)** Representative images and quantitative analysis of SA-β-gal activity after stimulation of the cells with Tyr for 1 week (N=3). Data are shown as the means ± SEM (**p*<0.05, ***p*<0.01, ***p<0.001 vs control).

Fig.5. Crosstalk between mTOR and p53 in Parkin-mediated mitophagy deficiency. (A) Analysis of p53 expression in cytosolic extracts of H9C2 cells stimulated with 500 µM Tyr for 72 h. GAPDH was used as a loading (N=3). **(B)** Cytosolic lysates of Ctrl and Tyr-treated cells for 72 h were immunoprecipitated with anti-Parkin, anti-p53 or control IgG antibodies, and immunoblotted with Parkin and p53 antibodies (N=3). **(C)** Analysis of p53 by immunoblot in cells transfected with SiScr or Sip53 siRNA for 48 h. Actin was used as a loading control (N=3). **(D)** Analysis of Parkin by immunoblot in mitochondrial extracts of H9C2 transfected with SiScr or Sip53 siRNA and stimulated with 500 µM Tyr for 72 h. VDAC was used as a loading control (N=3). **(E)** Analysis of LC3 and p62 by immunoblot in mitochondrial extracts of cells transfected with siScr or sip53 siRNA and stimulated with 500 µM Tyr for 72 h. VDAC was used as a loading control (N=3). **(F)** Analysis of p70S6K phosphorylation in Tyr-treated cells for 72 h in the presence or absence of 100 nM rapamycin (rapa) (N=3). **(F)** Analysis of p53 in cytosolic extracts of cells stimulated with 500 µM Tyr for 72 h in the presence of rapa, when indicated (N=3). GAPDH was used as a loading. Data are shown as the mean ± SEM (**p*<0.05, ***p*<0.01, ***p<0.001 vs control).

Fig. 6. Rapamycin treatment restores mitophagy preventing mitochondrial dysfunction, DDR and senescence induced by MAO-A. H9C2 cells were pre-treated with Vcle or rapamycin (rapa, 100 nM) and stimulated with 500 µM Tyr for 72 h. **(A)** Analysis of Parkin by immunoblot in mitochondrial extracts; VDAC was used as a loading control for mitochondria (N=3). **(B)** LC3 and p62 expression in mitochondrial fractions of cells; VDAC was used as a loading control (N=3). **(C)** mtDNA copy number (ND1/Actin) by real-time PCR (N=3). **(D)** Quantitative analysis of mitochondrial membrane potential with JC1 staining. **(E)** Representative images of mitochondrial 8-OH-dG immunostaining. **(F)** Analysis of total and pH2A.X by immunoblot in cells stimulated with Tyr for the indicated times. Actin was used as a loading control (N=3). **(G)** Analysis of p21 by immunoblot. Actin was used as a loading control (N=3). **(H)** Representative

ScholarOne, 375 Greenbrier Drive, Charlottesville, VA, 22901 Support: (434) 964 4100

images and quantitative analysis of SA-β-gal activity in cells stimulated with Tyr for 1 week (N=3). Data are shown as the means ± SEM. (*p<0.05, **p<0.01, *** p<0.001 vs control).

For Peer Review

ScholarOne, 375 Greenbrier Drive, Charlottesville, VA, 22901 Support: (434) 964 4100

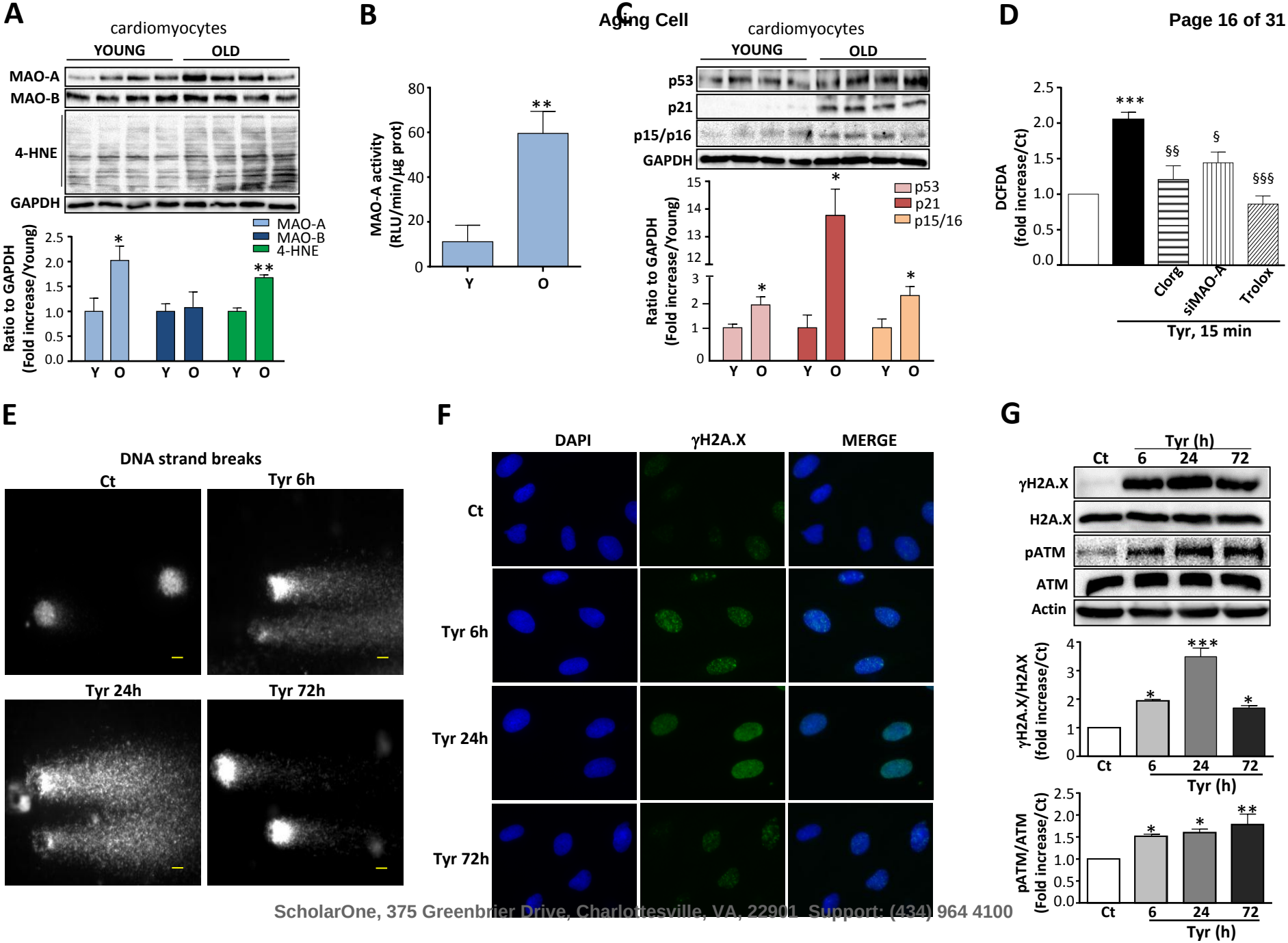

ScholarOne, 375 Greenbrier Drive, Charlottesville, VA, 22901 Support: (434) 964 4100

Figure 1

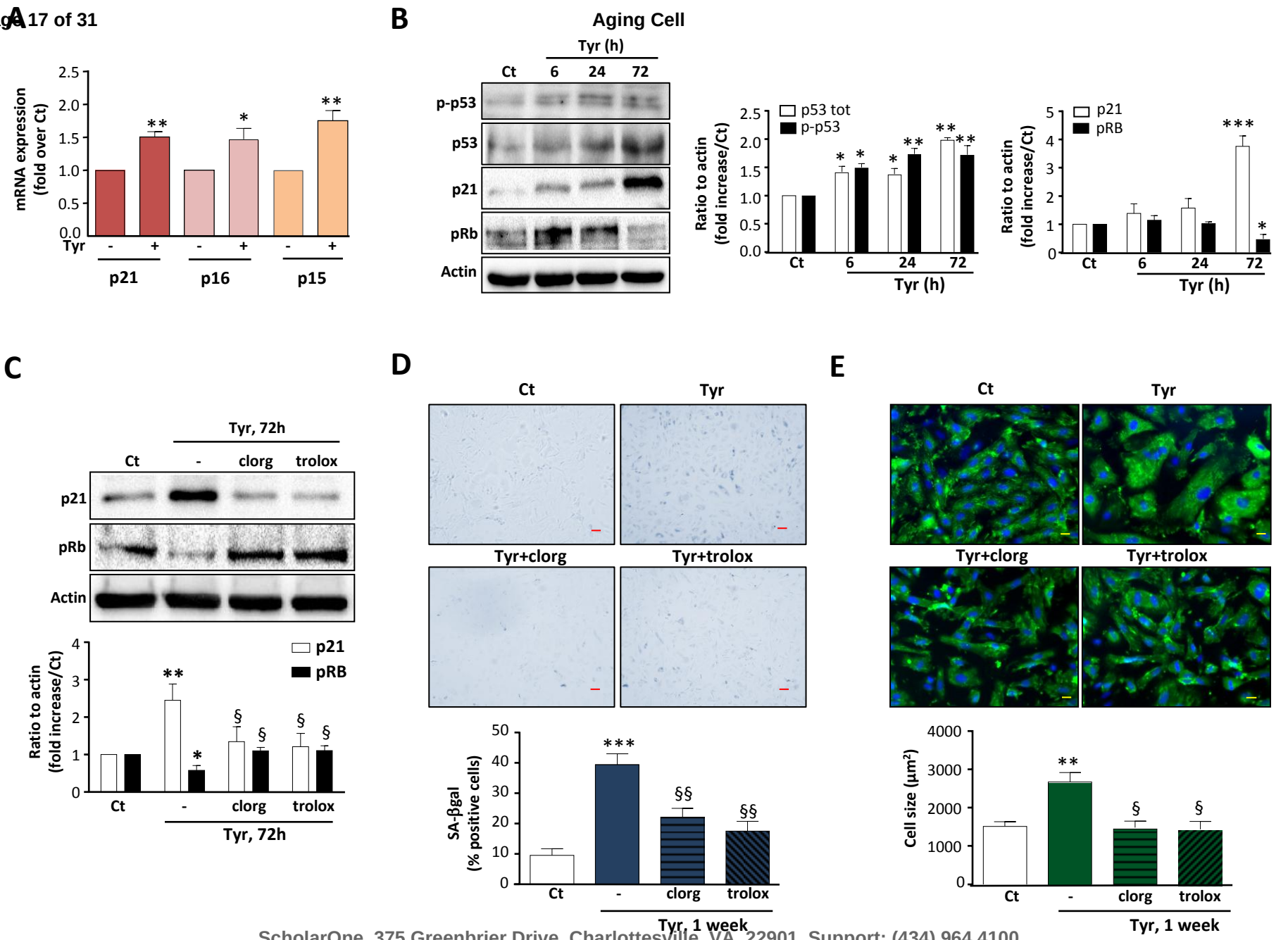

ScholarOne, 375 Greenbrier Drive, Charlottesville, VA, 22901 Support: (434) 964 4100

Figure 2

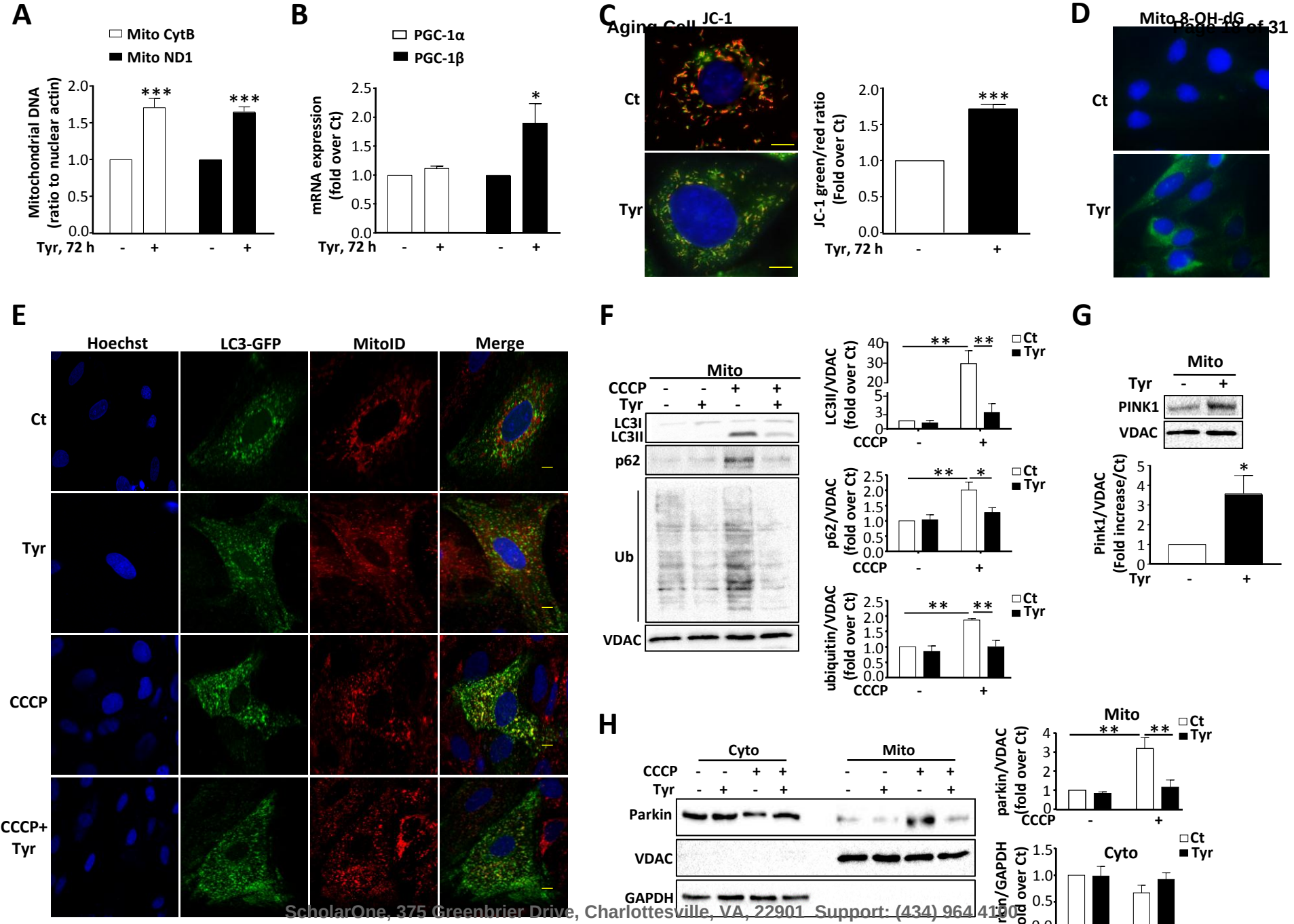

ScholarOne, 375 Greenbrier Drive, Charlottesville, VA, 22901 Support: (434) 964 4100

Figure 3

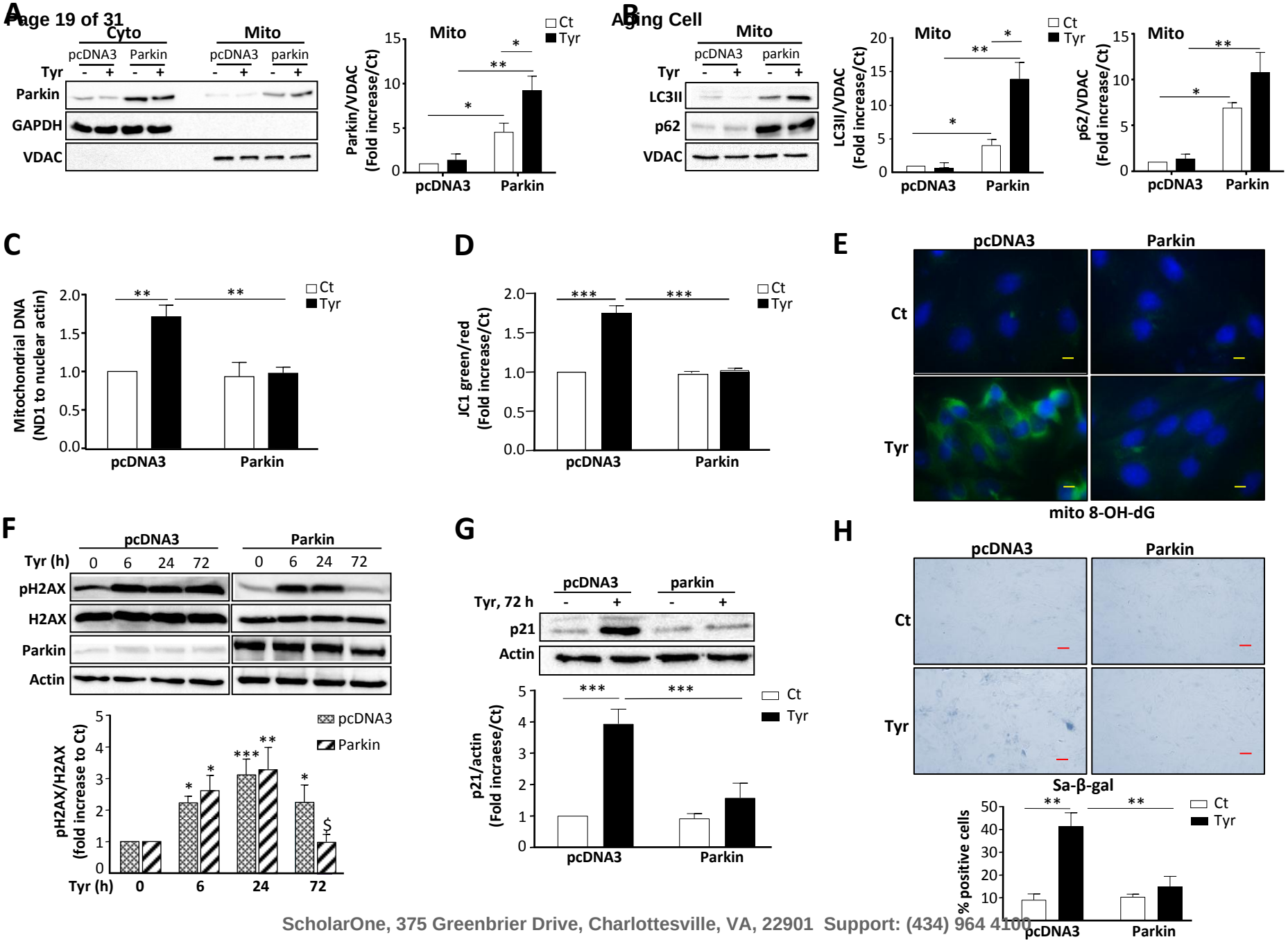

ScholarOne, 375 Greenbrier Drive, Charlottesville, VA, 22901 Support: (434) 964 4100

Figure 4

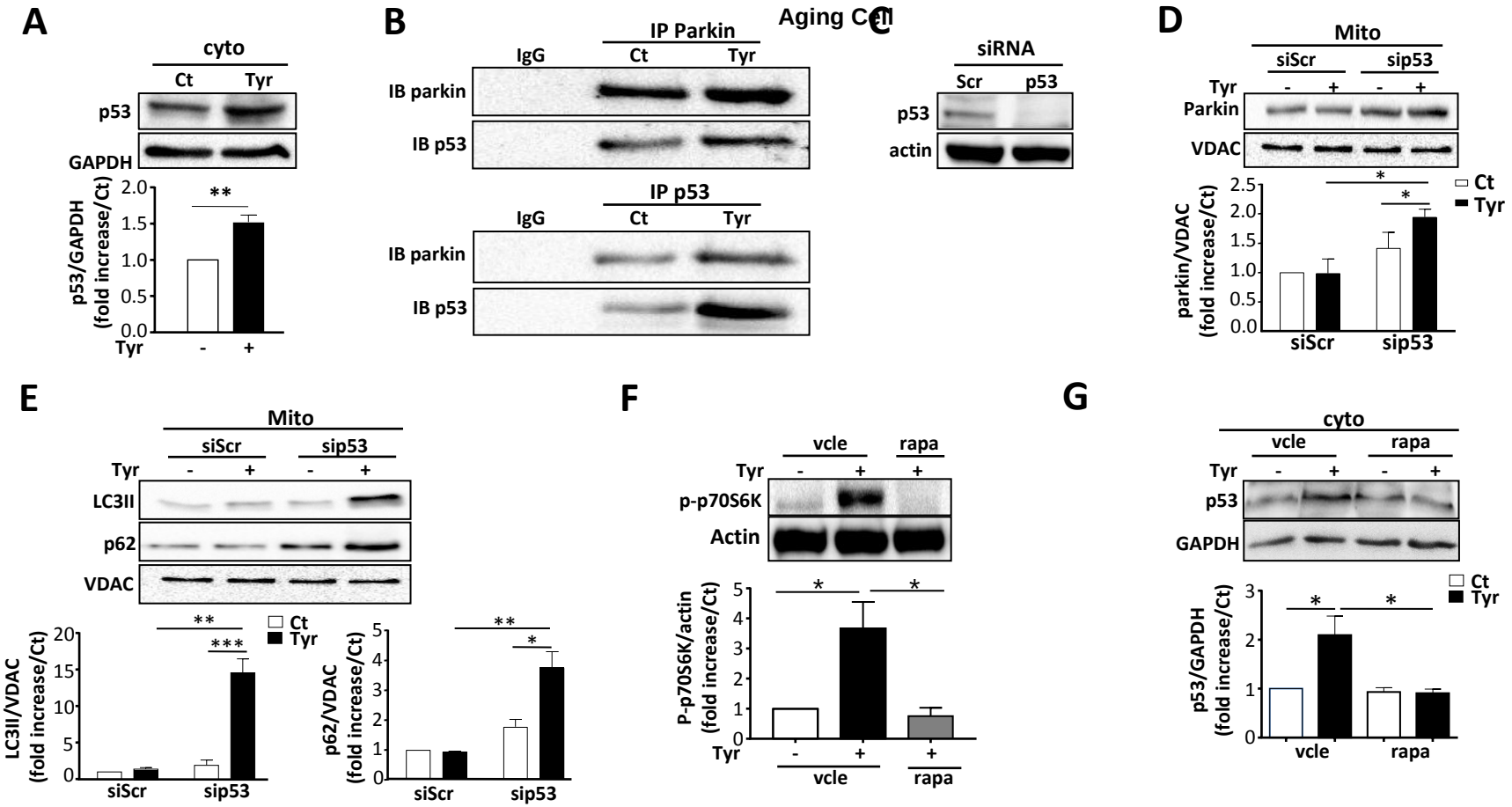
A
cyto
Ct
Tyr
p53
GAPDH
p53/GAPDH (fold increase/Ct)
Tyr
B
IP Parkin
IgG
Ct
Tyr
IB parkin
IB p53
IP p53
C
siRNA
Scr
p53
actin
D
Mito
siScr
sip53
Parkin
VDAC
parkin/VDAC (fold increase/Ct)
Ct
Tyr
E
LC3II
p62
LC3II/VDAC (fold increase/Ct)
p62/VDAC (fold increase/Ct)
F
vcle
rapa
p-p70S6K
Actin
P-p70S6K/actin (fold increase/Ct)
G
p53/GAPDH (fold increase/Ct)

Figure 5

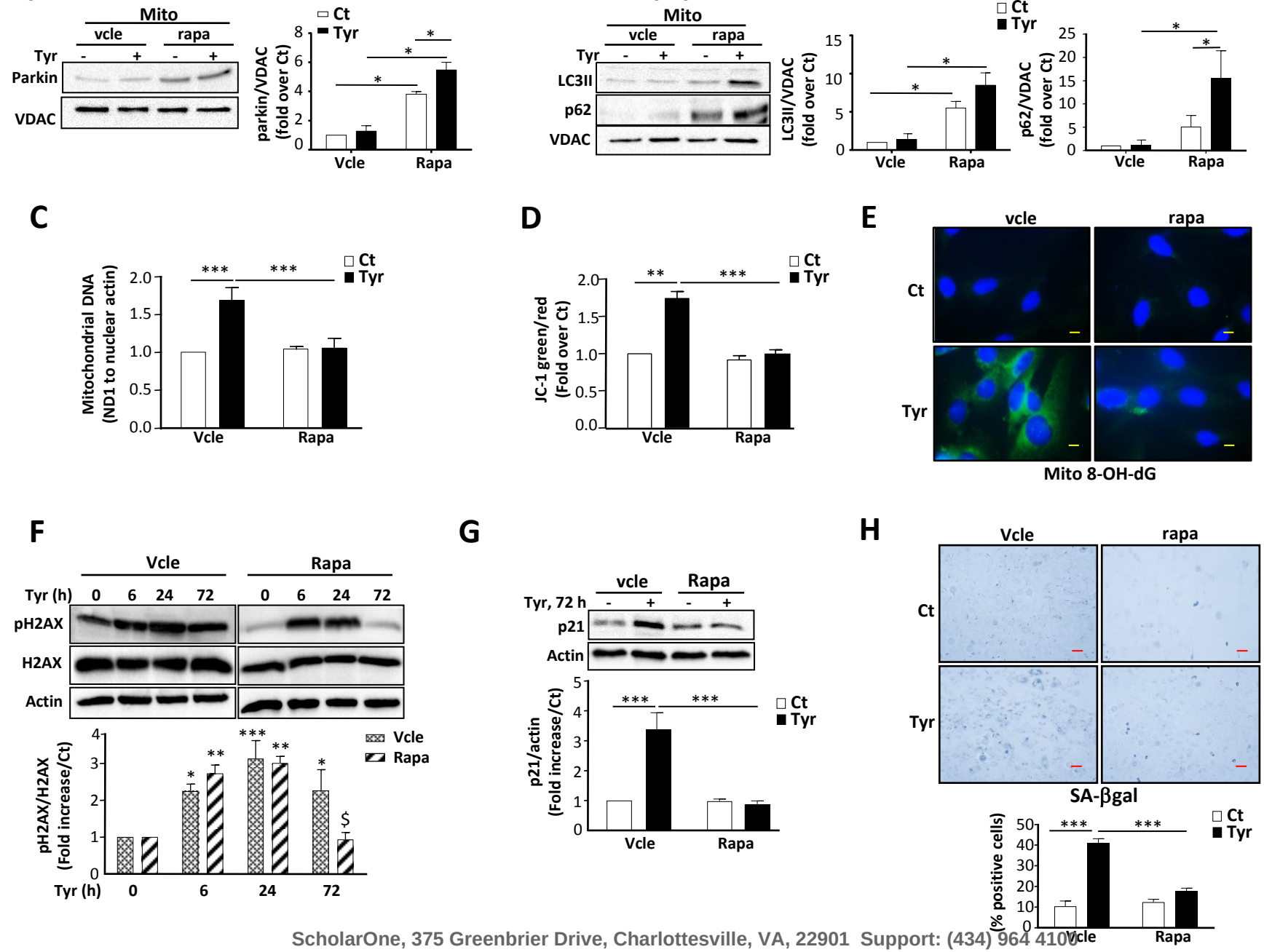

ScholarOne, 375 Greenbrier Drive, Charlottesville, VA, 22901 Support: (434) 964 4100

Figure 6

Material and methods

Cell proliferation rate

H9C2 cells were seeded in 6-well plates and various treatments were added to the medium during 1 week. After removal of the medium, the cells were harvested by trypsinization and plated at a density of $5x10^4$/well in fresh culture medium and the proliferation rate was evaluated by counting the cells at indicated times.

Cell Viability and Cell Death Assay

To evaluate cell viability, MTT ((3–4,5-dimethylthiazol-2-yl)-2,5-diphenyltetrazolium bromide; Sigma) was added for 3 h at 37°C and, after addition of DMSO, absorbance was read at 550 nm. For quantitative assessment of necrosis, LDH released in culture medium was measured using LDH cytotoxicity Assay Kit according to the manufacturer's instructions (Biovision). Apoptosis was measured as caspase-3 activation using a commercial kit (Biotium) according to the manufacturer's instructions.

Mitochondrial ROS and H_2O_2 measurements

The mitochondrial ROS was measured by mitoSOX probe (Invitrogen, Molecular Probes). Briefly, the cells were loaded with mitoSOX probe at a final concentration of 5 µM and incubated for 30 min after the indicated treatments. Cells were resuspended in HBSS before reading to Tecan plate reader. Extracellular H_2O_2 detection was evaluated by Amplex-Red probe (Invitrogen, Molecular Probes) on cell supernatants collected and mixed with an Amplex red solution.

Figure legends

Supplementary Figure 1

(A) Immunoblots of MAO-A expression in scramble-siRNA (Scr) or MAO-A-siRNA-transfected cells with actin as a loading control. (N=3). **(B)** H_2O_2 measurements in the extracellular media with Amplex RED probe in response to 500 μM Tyr, and in the presence of clorg (10 µM), MAO-A siRNA or Trolox (500 µM), when indicated (N=3). **(C)(D)(E)** Measurements of MTT, Lactate Dehydrogenase release in culture media and caspase-3 activity in cells treated with 500 µM Tyr for 24 h (N=3). NS, non statistical. **(F)** Proliferation rate of H9C2 evaluated at indicated times after 7d treatment with 500 µM Tyr in the presence of clorg (10 µ*M*) or Trolox (500 µ*M*), when specified (N=3). Data are shown as the means ± sem (**p*<0.05, ***p*<0.01, ***p<0.001 vs control).

Supplementary Figure 2

(A) DCFDA oxidation in response to 100 μM NE for 15 min, and in the presence of clorg (10 µM), siMAO-A siRNA or Trolox (500 µM), when indicated (N=3). **(B) (C)** Measurements of MTT and Lactate Dehydrogenase release in culture media in cells treated with 100 µM NE for 24 h (N=3). NS, non statistical. **(D)** Immunoblots of total and phosphorylated levels of H2A.X in cell extracts after stimulation with NE (100 µM) for the indicated time. Actin was used as loading control. Quantifications of the ratios of phospho-H2A.X on total H2A.X are shown in the lower panel (N=3). **(E)** Analysis of mRNA levels of CDKi p21, p16 and p15 normalized to GAPDH by real-time RT-PCR in cells stimulated with 100 µM NE for 72 h (N=5). **(F)** Immunoblots of phospho(Ser15)p53, total p53, p21 and pRb in cells stimulated with 100 µM NE for 6 to 72 h. Quantifications of the ratios to actin are shown on the histogram below (N=3). **(G)** Immunoblots of p21 and pRb in cells stimulated with 100 µM NE for 72 h and pretreated with clorg or trolox, when specified. Quantifications of the ratios to actin are shown on the histogram below (N=3).

Supplementary Figure 3

For Peer Review

(A) Representative images and quantitative analysis of SA-β-gal activity in cells stimulated with 100 µM NE for 1 week in the presence of clorg (10 µM) or Trolox (500 µM), when indicated. The number of blue cells was counted and expressed as percent of total cell number. For each condition, a total of 100 cells were counted (N=3). **(B)** Representative images and quantitative analysis of cell area after stimulation with 100 µM NE for 1 week in the presence of clorg (10 µM) or Trolox (500 µM), when indicated. DAPI (blue) was used to label nucleus and Vinculin for cell size measurement (green). Scale Bar= 10 µm. For each condition, a total of 100 cells were counted (N=3). **(C)** Proliferation rate of H9C2 evaluated at indicated times after 1 week of treatment with 500 µM Tyr in the presence of clorg (10 µ*M*) or Trolox (500 µ*M*), when specified (N=3). Data are expressed as means ± sem (***p*<0.01, ***p<0.001 vs control; §*p*<0.05, §§*p*<0.01 vs Tyr).

Supplementary Figure 4

(A) Mitochondrial ROS with mitoSOX probe in H9C2 treated with 500 µ*M* Tyr for 72h. **(B)** Analysis of LC3 and p62 levels by immunoblot in cells stimulated with 500 µ*M* Tyr for 72h. Actin was used as a loading control (N=3). **(C)** Analysis of Parkin levels by immunoblot in cells stimulated with 500 µ*M* Tyr for 72h. Actin was used as a loading control (N=3). Data are shown as the means ± SEM. (***p<0.001 vs control).

Supplementary Figure 5

(A) Analysis of Parkin levels by immunoblot in cells transfected with pcDNA3 or Parkin and stimulated with 500 µM Tyr for 72h. Actin was used as a loading control (N=3). **(B)** Analysis of Parkin levels by immunoblot in cytosolic extracts from cells transfected with pcDNA3 or Parkin and stimulated with 500 µM Tyr for 72h. GAPDH was used as a loading control (N=3). **(C)** Mitochondrial ROS with mitoSOX probe in H9C2 transfected with pcDNA3 or Parkin and treated with 500 µ*M* Tyr for 72h (N=5). **(D)** Analysis of MAO-A levels by immunoblot in cells transfected with pcDNA3 or Parkin and stimulated with 500 µM Tyr for 72h. Actin was used as a loading control (N=3). Data are shown as the means ± SEM. (*p<0.05, ***p<0.001 vs control).

Supplementary Figure 6

(A) Analysis of Parkin levels by immunoblot in cytosolic extracts from cells pre-treated with rapamycin and stimulated with 500 µM Tyr for 72h. GAPDH was used as a loading control (N=3). **(B)** Mitochondrial ROS with mitoSOX probe in H9C2 pre-treated with rapamycin and stimulated with 500 µM Tyr for 72h (N=5). Data are shown as the means ± SEM. (***p<0.001 vs control).

Supplementary Figure 7

Schematic representation of MAO-A-induced senescence signaling pathway**.** MAO-A-induced H_2O_2 generation causes mitochondrial oxidative damage and ROS generation leading to DDR and activation of the p53/p21 pathway. Accumulation of p53 in the cytoplasm through mTOR activation impairs mitochondrial quality control, leading to further accumulation of damaged mitochondria within an amplification loop that stabilizes DDR and senescence.

For Peer Review

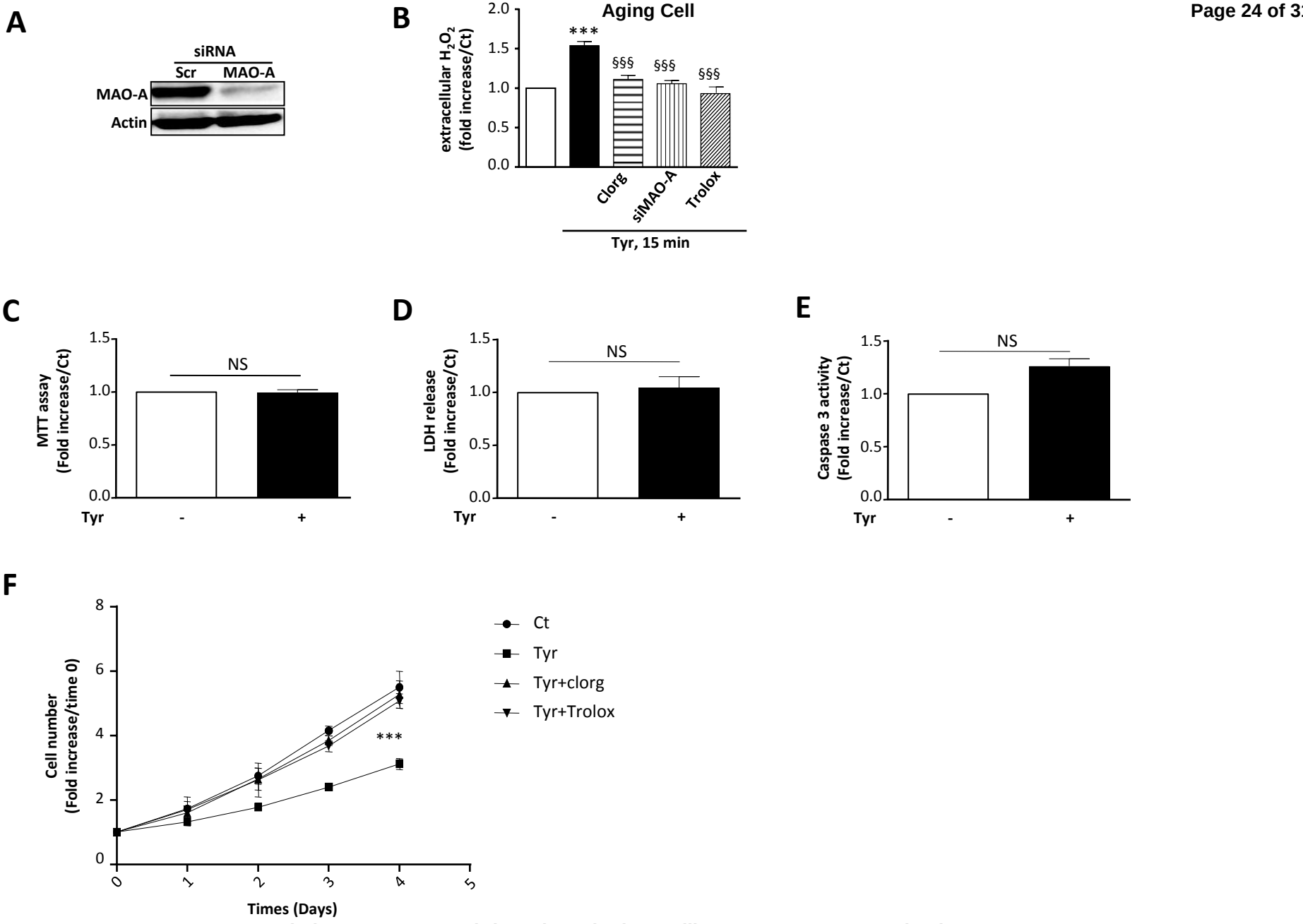

Supplementary Fig 1

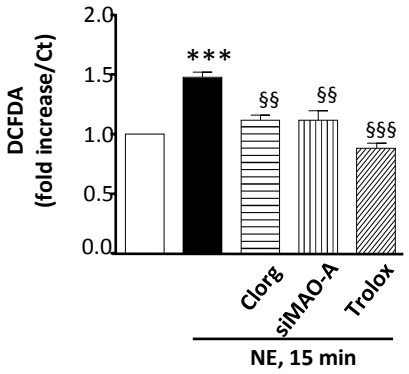
A
DCFDA
(fold increase/Ct)
2.0
1.5
1.0
0.5
0.0
***
§§
§§
§§§
Clorg
siMAO-A
Trolox
NE, 15 min

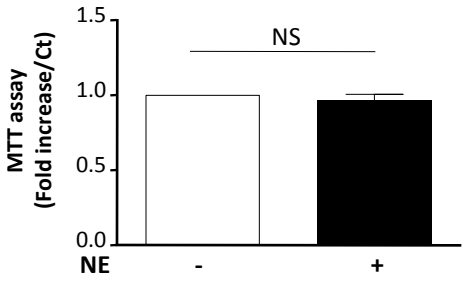
B
MTT assay
(Fold increase/Ct)
1.5
1.0
0.5
0.0
NS
NE
-
+

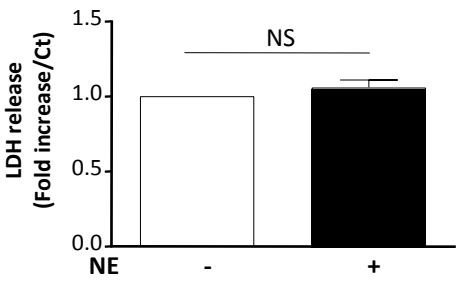
C
LDH release
(Fold increase/Ct)
1.5
1.0
0.5
0.0
NS
NE
-
+

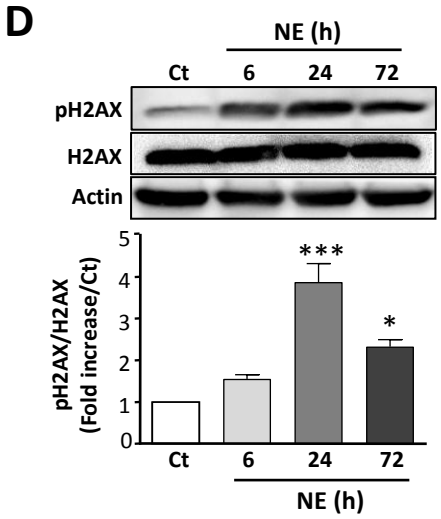
D
NE (h)
Ct
6
24
72
pH2AX
H2AX
Actin
pH2AX/H2AX
(Fold increase/Ct)
5
4
3
2
1
0
***
*
Ct
6
24
72
NE (h)

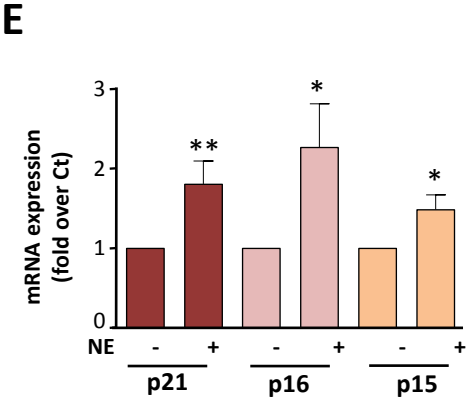
E
mRNA expression
(fold over Ct)
3
2
1
0
**
*
*
NE
-
+
-
+
-
+
p21
p16
p15

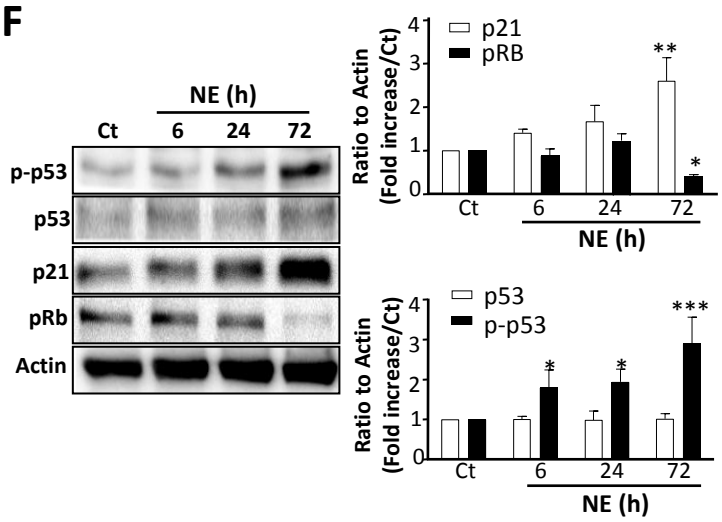
F
NE (h)
Ct
6
24
72
p-p53
p53
p21
pRb
Actin
Ratio to Actin
(Fold increase/Ct)
p21
pRB
**
*
Ct
6
24
72
NE (h)
p53
p-p53
***
*
*
Ct
6
24
72
NE (h)

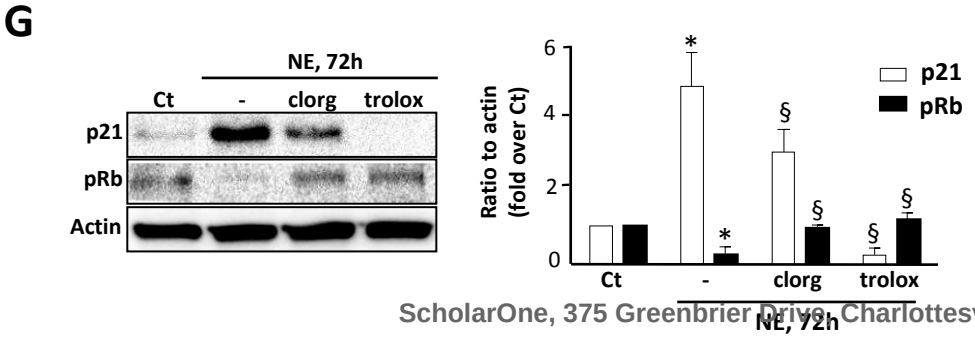
G
NE, 72h
Ct
-
clorg
trolox
p21
pRb
Actin
Ratio to actin
(fold over Ct)
6
4
2
0
*
*
§
§
§
§
p21
pRb
Ct
-
clorg
trolox
NE, 72h

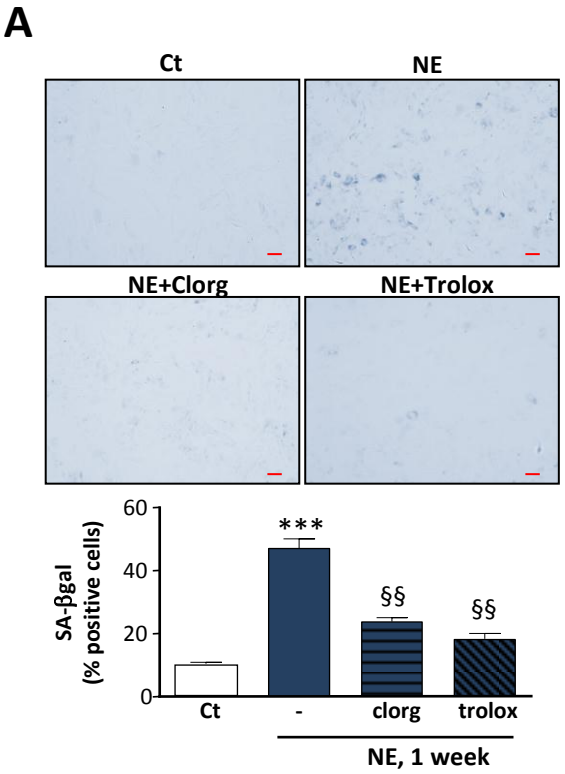

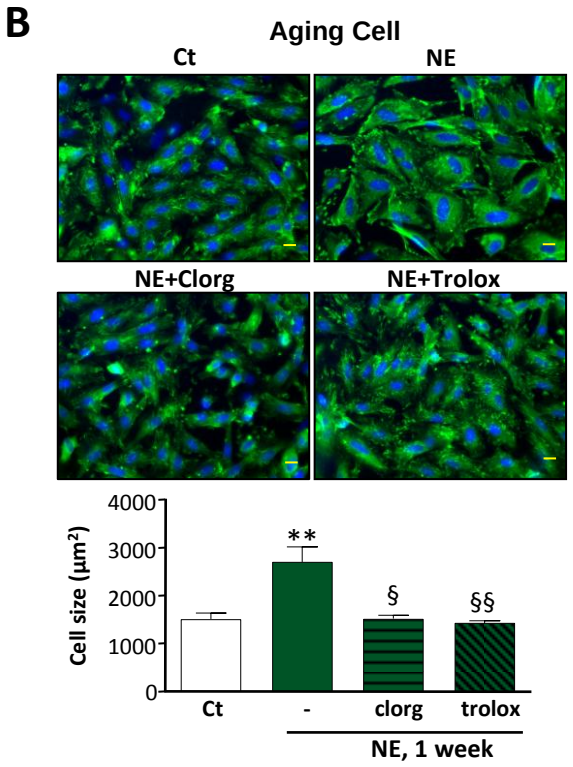

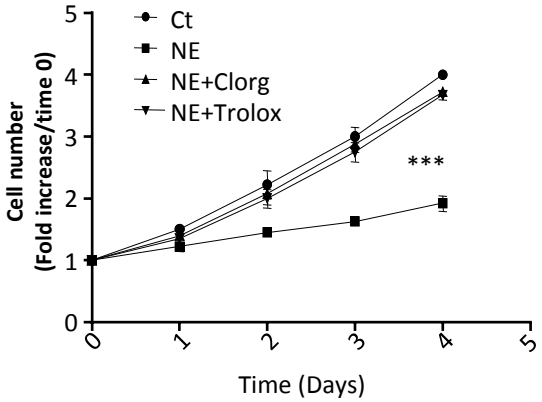

Supplementary Fig 3

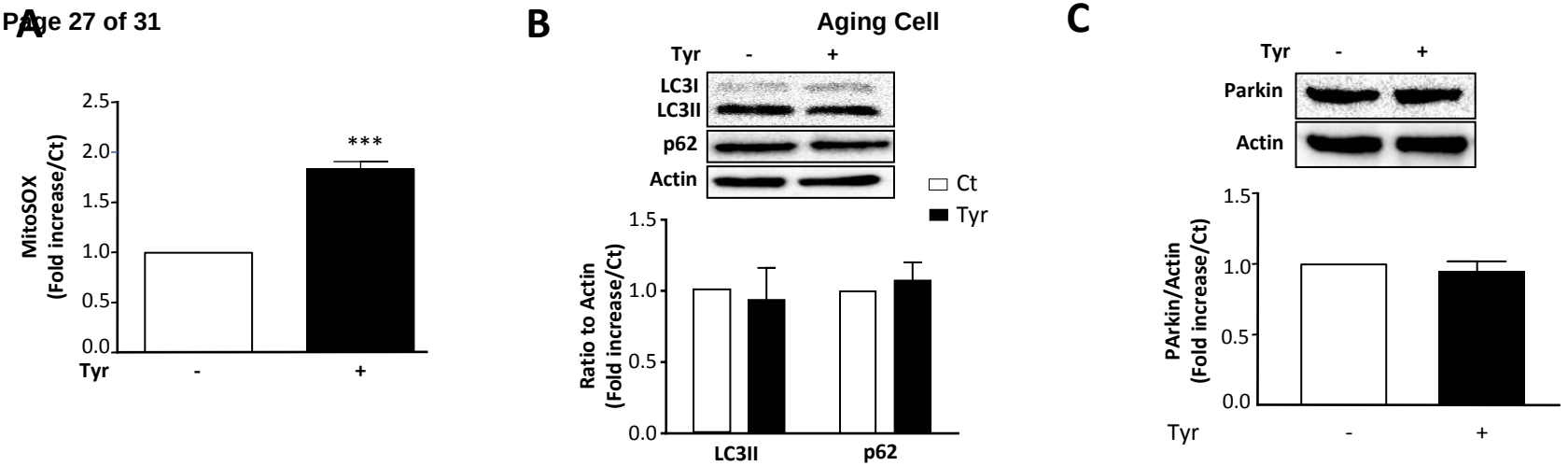

Supplementary Fig 4

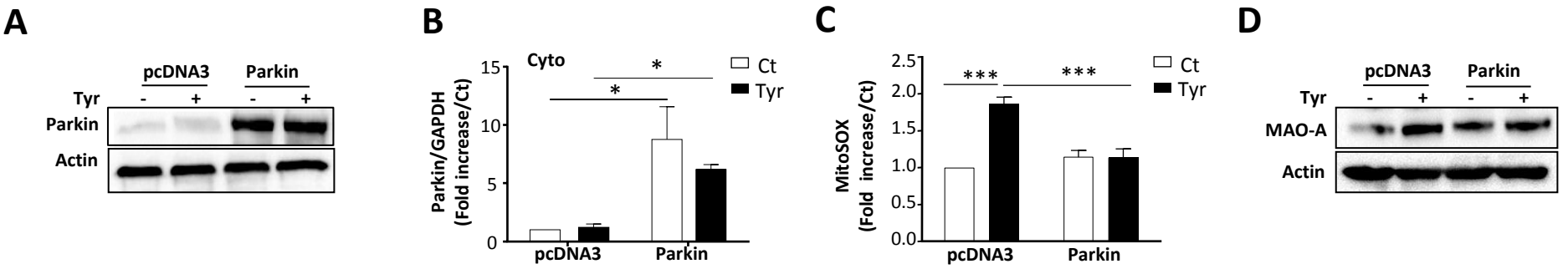

Supplementary Fig 5

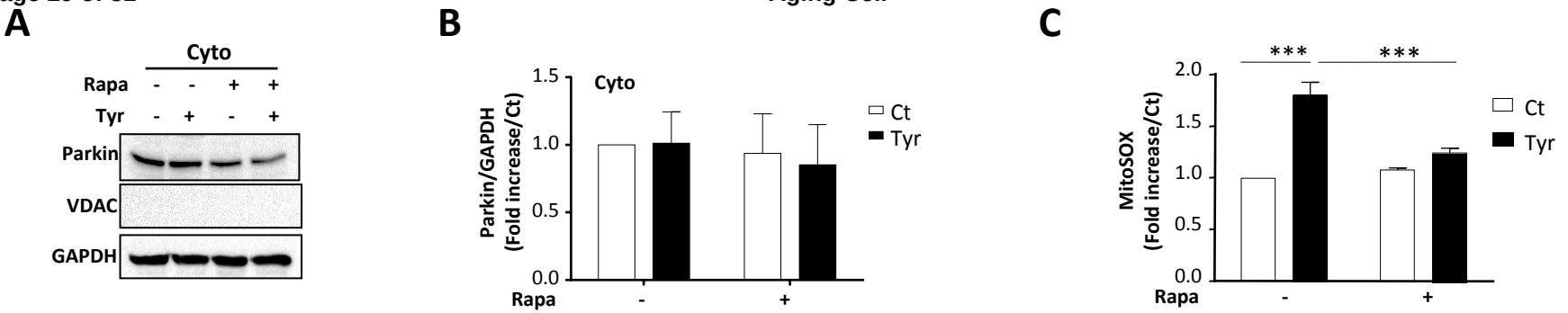

Supplementary Fig 6

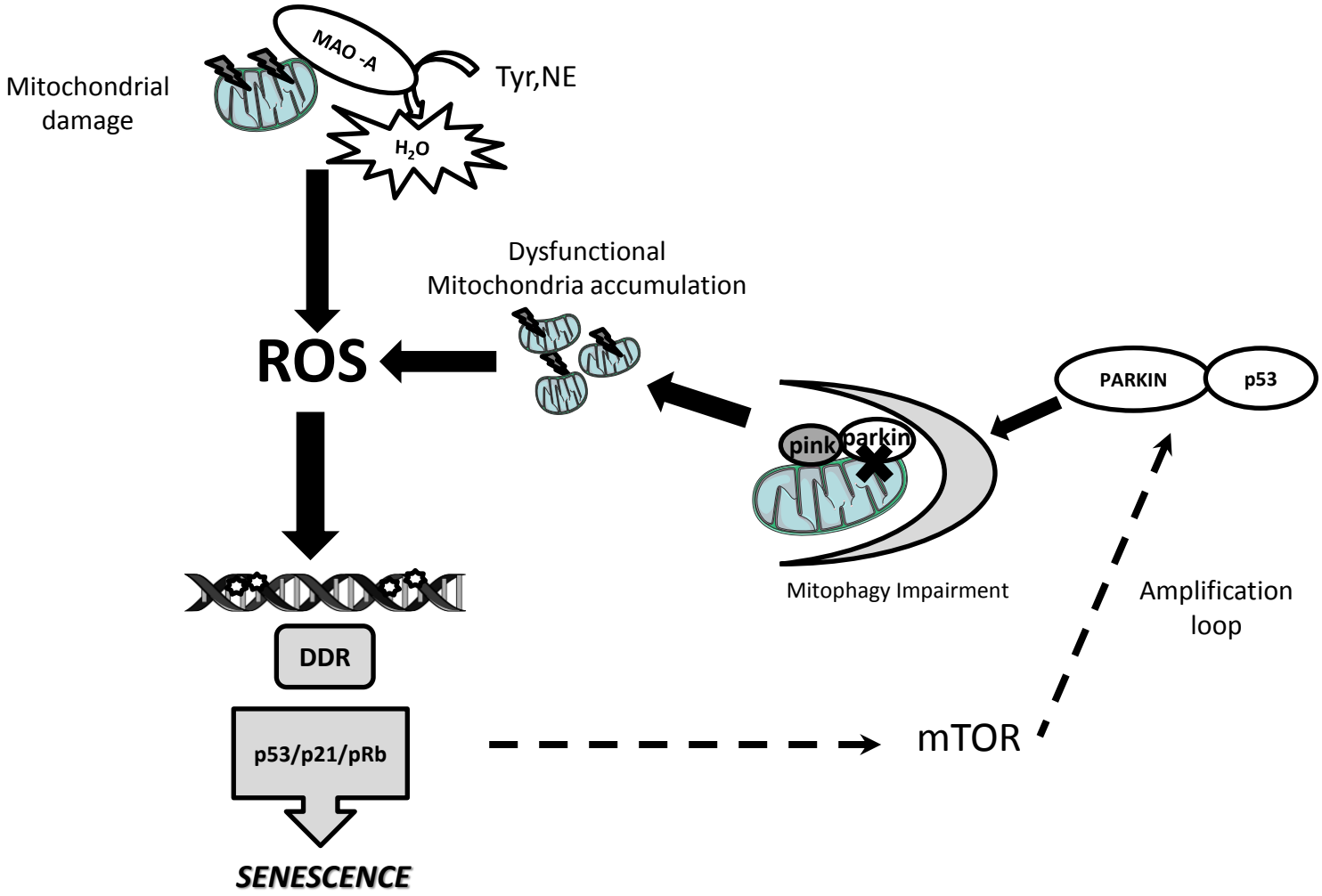

Supplementary Fig 7

AGING CELL AUTHOR CHECKLIST. *Authors should submit this checklist together with their manuscript. Please ensure that you have read the Author Guidelines in detail before submission.*

Title	Monoamine oxidase-A is a novel driver of stress-induced premature senescence through inhibition of parkin-mediated mitophagy
Authors	Nicola Manzella, Damien Maggiorani, Yohan Santin, Hélène Martini, Victorine Douin-Echinard, Joao F. Passos, Frank Lezoualc'h, Claudia Binda, Angelo Parini and Jeanne Mialet-Perez
Manuscript Type	Original article
Total Character Count (including spaces)[1]	50657
Word count of Summary[2]	242
Number of papers cited in the References[3]	38
Listing of all Tables (Table1, Table 2 etc)[4]	

Figure specifications (please complete one row per figure)[5] *Figure no.*	Colour *(yes/no)*	Greyscale *(yes/no)*	Black and white *(yes/no)*	Single column (80mm) *(yes/no)*	Double column (167mm) *(yes/no)*	Size of figure at full scale (mm x mm) *(insert details)*	Smallest font size used in the figure at full scale (minimum 6pt) *(insert details)*
1	yes				yes		
2	yes				yes		
3	yes				yes		
4	yes				yes		
5	no				yes		
6	yes				yes		

[1] The maximum character count allowed is 50,000 (incl. spaces) for Primary Research Papers and Reviews, 10,000 for Short Takes.

[2] Summary should not exceed 250 words.

[3] Primary Research Papers can contain a maximum of two tables. If more are needed they should replace some of the Figures or can be placed in the Supporting Information.

[4] A maximum of 45 references is allowed for Primary Research Papers and 20 references for Short Takes.

[5] A Primary Research Paper may contain up to 6 figures and a Short Take up to 2 figures. Authors are encouraged to provide figures in the size they are to appear in the journal and at the specifications given.

For Peer Review